Journal for Occultation Astronomy

Volume 10 · No. 2 2020-02

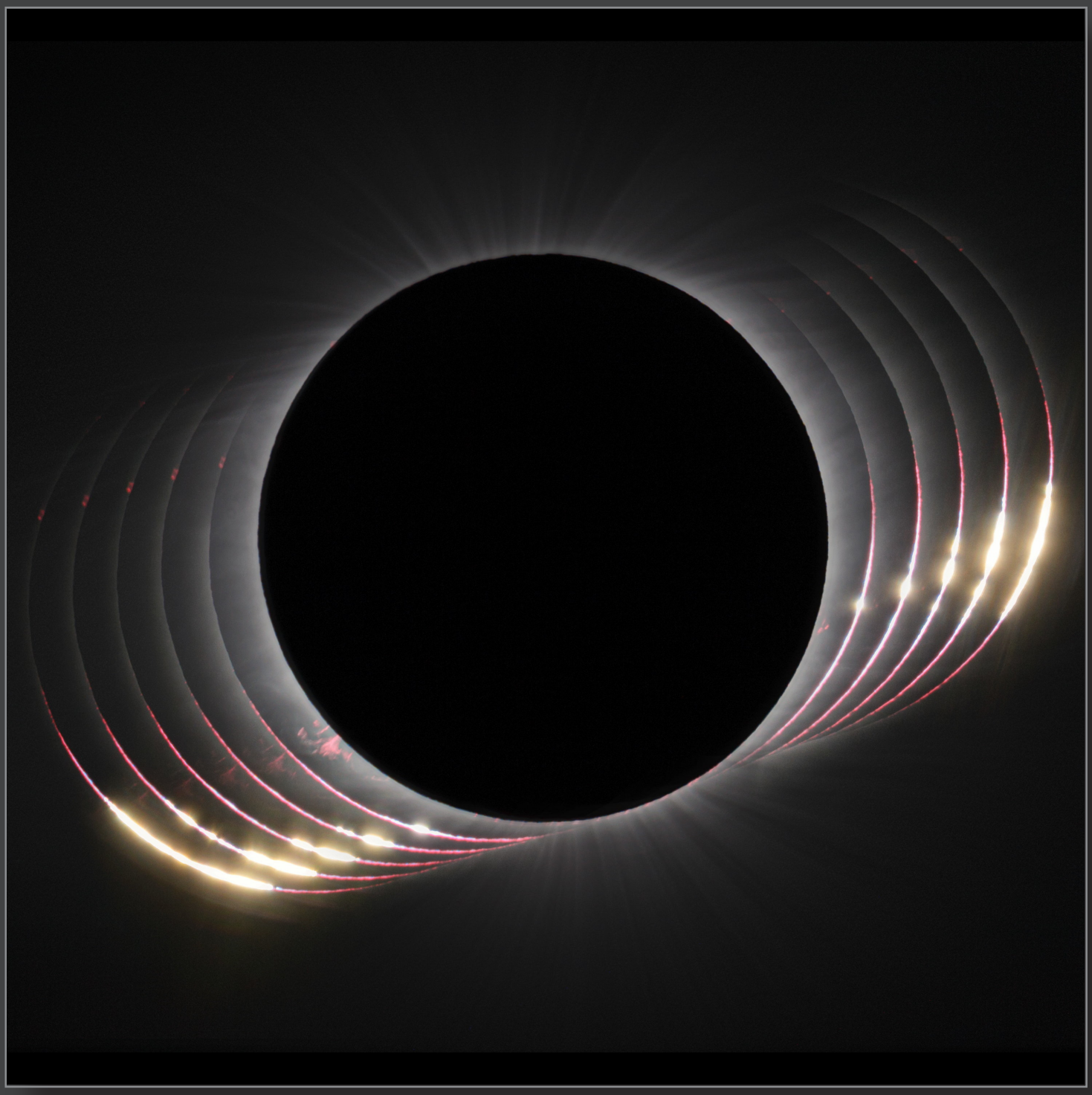

Baily's Beads and the Solar Diameter

Dear reader,

With the publication of this issue of *Journal for Occultation Astronomy* many parts of the world are locked down by health precautions due to the COVID-19 virus. Public observatories with thier medium-sized telescopes, one of the major pillars of occultation science, are temporarily shut down.

So it is now the time for occultation observers who have equipment of their own to keep observing and make contributions to science. Over many years our digital network of predictions, reports and evaluation of occultations has reached a high level and works very well. The RASNZ meeting TTSO goes virtual this year to exchange experiences and results.

This issue of *JOA* presents some observational projects which are within the reach of smaller telescopes. Alex Pratt discovered a possible double star and Konrad Guhl measured the solar diameter with a 4-inch telescope during a solar eclipse. Just before the virus crisis occultation observers met for a workshop and took the first steps into high-precision-timing with a digital camera. Testing the reliability of NTP timing is still a task for clouded nights and Chiron, far beyond Jupiter, reminds us of many objects in the outer Solar System to be measured with the help of occultations. Many things can be done - even in these difficult days.

In a slight variation of an old saying in Britain: *"Keep well and carry on with chasing the shadows!"*

Oliver Klös

Oliver Klös
IOTA/ES, Public Relations

JOA Volume 10 · No. 2 · 2020-2 $ 5.00 · $ 6.25 OTHER (ISSN 0737-6766)

In this Issue:

COVER

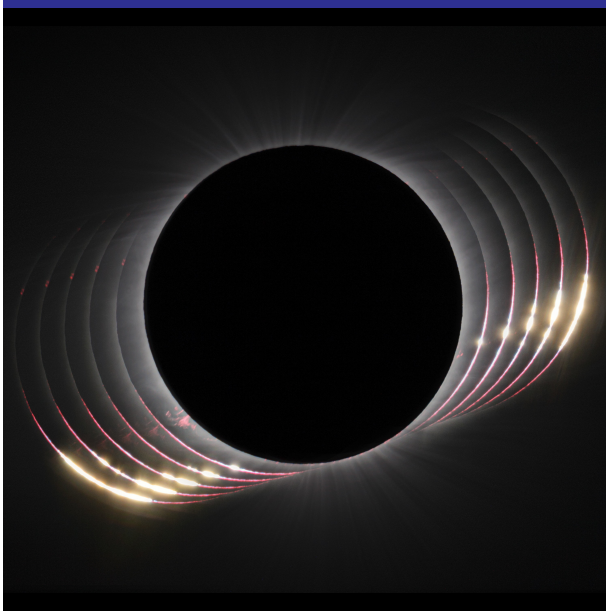

The cover highlights Baily's Beads, a feature of total solar eclipses which are measured by occultation observers to record variations of the solar diameter. It's composed of a series of images taken during a total solar eclipse visible from ESO's La Silla Observatory on 2019 July 2.

Credit: Petr Horálek, ESO
https://www.facebook.com/PetrHoralekPhotography

Copyright Transfer

Rules for Authors

In order to optimize the publishing process, certain rules for authors have been set up how to write an article for *JOA*. They can be found in "How to Write an Article for *JOA*" published in this *JOA* issue (2018-3) on page 13. They also can be found on our webpage at http://www.iota-es.de/how2write_joa.html .

Journal for Occultation Astronomy

Baily's Beads Observations during the Total Solar Eclipse 2019 July 2

Konrad Guhl • IOTA/ES • Archenhold-Sternwarte • Berlin • Germany • kguhl@astw.de

ABSTRACT: The timing of Baily's beads, observed during a solar eclipse, is one of the most accurate ground-based methods for estimating the solar radius. This work presents the observation and the result of the beads measurements derived from an expedition to the northern edge of totality of the total solar eclipse on 2019 July 2. A correction to the solar radius of ΔR_s = -0.08'' ± 0.06'' was derived from this observation.

Introduction

Measuring the angular solar diameter (enabling one to derive the physical diameter if the Earth-Sun distance is known) has been a fundamental challenge for astronomers for more than two thousand years. After micrometric, heliometric or transit measurements, astronomers found one of the best ground-based methods for measuring the solar diameter: the observation of the disappearance and reappearance of the remaining sunlight in valleys on the lunar limb during a total (TSE) or annular solar eclipse (ASE). As Francis Baily (1774-1844) was one of the first who described these tiny points of light on the lunar edge during a total eclipse, the technique was named Baily's beads observation. Such observations have been a focus of IOTA and IOTA/ES activities for many years. The aim was the measurement of the solar diameter and detection of possible variations of it.

Method

To observe the disappearance / reappearance of the beads, the observer is sited near the edge of totality (but inside the totality zone) and records the eclipse with a camera, together with some kind of time information – very similar to the recording of stellar occultations by the Moon or asteroids. The movie (video file or image sequence, depending on the recording system) is inspected visually, and the time of disappearances and reappearances of any beads are noted. To describe these beads as observation points they must be identified along the Moon's edge by using the axis angle (AA) of the limb feature which caused the bead. The axis angle is measured from Moon's north pole towards the east. Figures 1 (a-f) shows six single frames between 20h 39m 57.5s and 20h 40m 09.7s UTC of the TSE observation on 2019 July 2. Figure 1a shows the area from AA 9° to 27°. Three beads at AA = 21.7°, AA = 18.4° and AA = 11.4° are formed in this time. Figure 1f only the bead at AA = 11.4° remains. It disappears at 20h 40m 1 1.2s UTC. To identify the disappearance and reappearance of these beads the *Baily Bead Analysis* tool of *Occult* software [1] can be used for the prediction and a simulation. Version 4.5.3.0 of *Occult*, used for this analysis, contains both LRO (Lunar Reconnaissance Orbiter) LOLA and Kaguya LALT space mission data as most accurate data about the limb profile of the Moon.

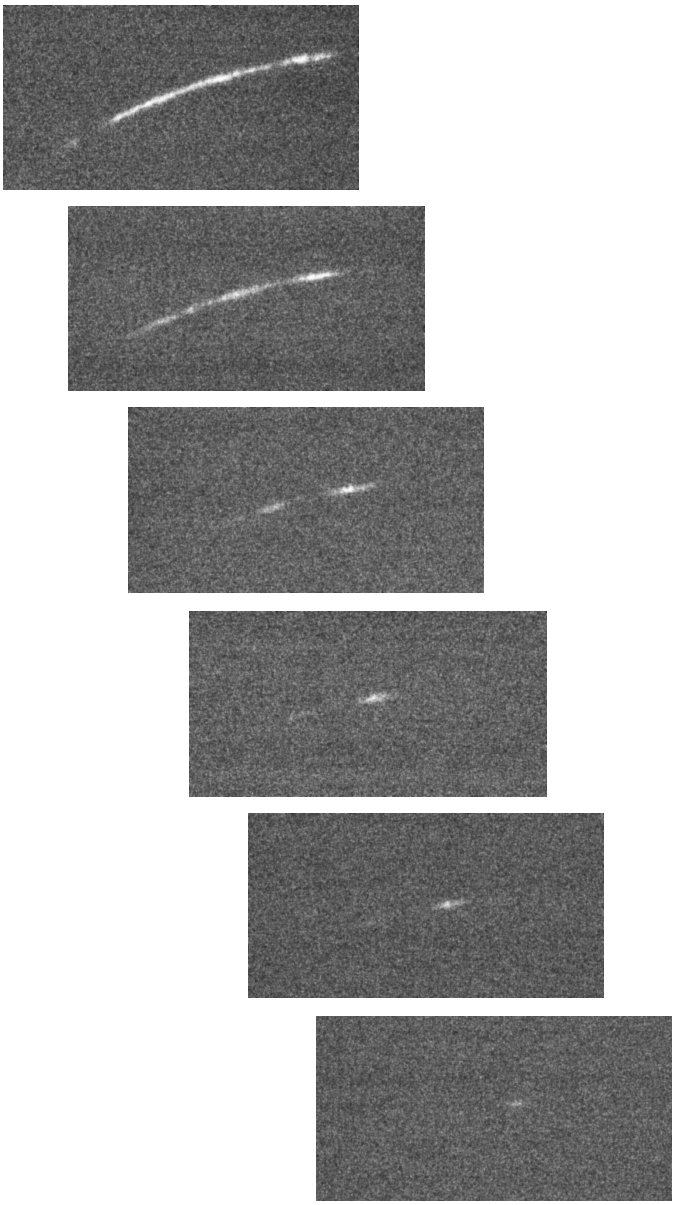

Figure 1 (a-f). A sequence of images of the 2019 July 2 TSE, showing the appearance and disappearance of three beads (at AA = 21.7°, 18.4° and 11.4°).

After this identification of disappearing / reappearing beads and entering the corresponding times into *Occult's Baily Bead Analysis* tool, the differences of the Moon's limb and the Sun's limb from the mean limb profile are calculated and displayed by *Occult* for this bead and for this observed time. The difference of these two values can be interpreted as a correction to the solar radius. This process is repeated for all beads.
See also [2] for a more detailed explanation of the method.

Limb Darkening Function

The visual solar limb is the inflection point in the limb darkening function (LDF), i.e. brightness vs. solar radius. To register the inflection point in the LDF is the guarantee to observe the real visual solar limb. Therefore the adjustment of the camera parameters, like Gain, dynamic range and exposure time are important. The LDF can be obtained from an intensity profile in a single frame along the Sun radius. Figures 2a, b show such profiles from observation with 8-bit image depth (2017) and 12-bit image depth (2019), which shows the advantage of 12-bit depth in the dynamic range of signal.
Because the inflection point of LDF varies with the wavelength of the light a bandpass filter must be used. The derived solar radius is then valid for this wavelength.

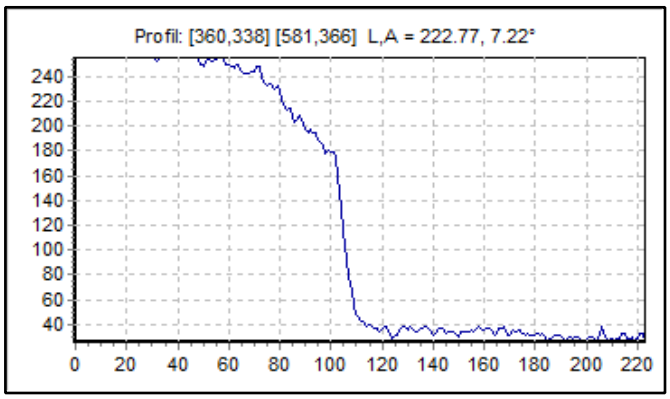

Observation Campaign and Eclipse Circumstances

In 2019, IOTA/ES organized an expedition to the northern edge of the total solar eclipse on July 2, where bead observations were possible. Additionally, some US observers (IOTA) observed this event; a separate report is anticipated. The TSE02072019 eclipse path crossed the Pacific Ocean and South America (Figure 3). The most western observation place (highest height) was in Chile, where the complete zone including both rims was observable. At the coast of the Pacific Ocean the maximum height of the Sun during totality was approximately 13°.
In collaboration and prior consultation with the American team, the IOTA/ES expedition targeted the northern edge for beads observation. Observations on the southern edge were made by Joan and David Dunham (IOTA); Richard Nugent (IOTA) observed on the central line.
Due to the expected marine layer over the Pacific Ocean, the observation point was selected near the crossing of the Pan Americana highway and the northern edge. The next village from this point is Domeyko (Figure 5), on the southern edge of the

Figures 2a, b. Limb darkening functions (LDF) derived from an 8-bit depth video frame in 2017 (left) versus a LDF derived from a 12-bit depth image in 2019 (bottom). The x-axis is in pixels, the y-axis gives the intensity values.

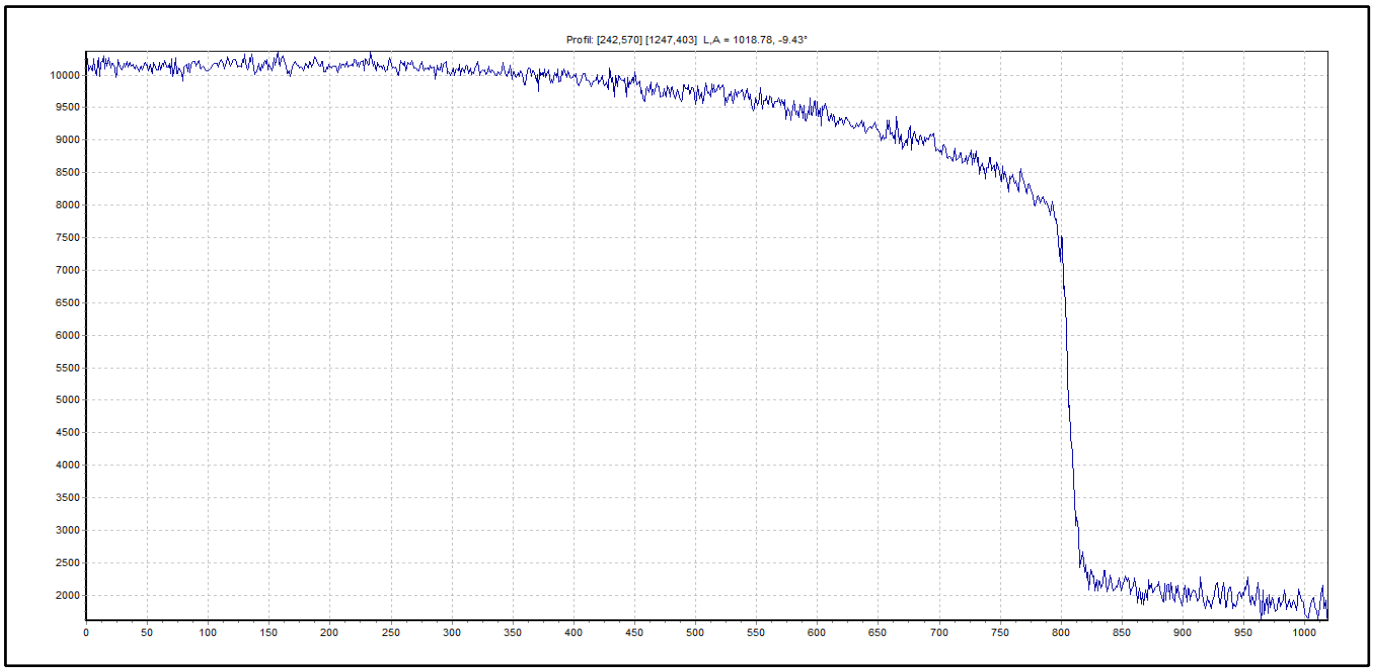

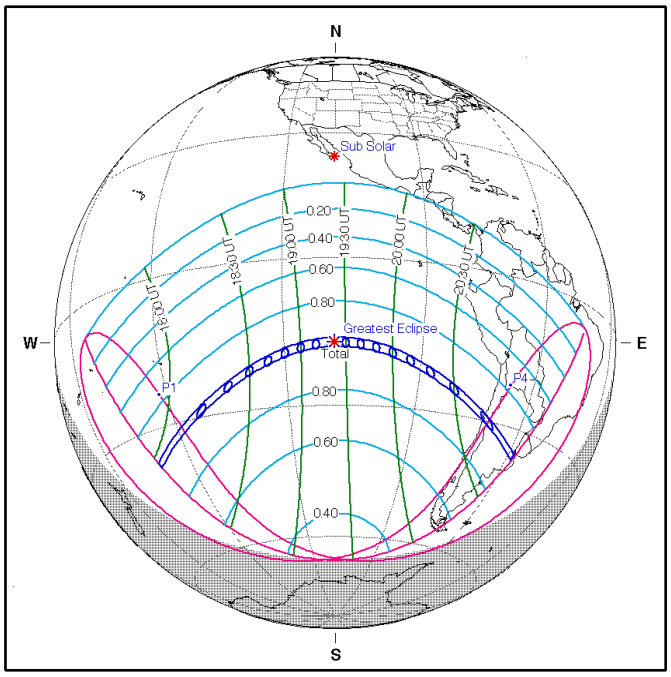

Figure 3. Area of visibility of the solar eclipse (from [3]).

Atacama Desert. After the eclipse, "Pretty picture" observations by many people proved the fear of the marine layer was unwarranted. Choosing a place in the desert with rocks and the low altitude of the Sun ensured that the air mass was huge and air scintillation was massive.

Observations

With the observation of TSE02072019, the observation technique was changed from a video camera with 8-bit depth to a camera recording images with 12-bit depth and storing them in FITS format. Like previous TSE and ASE observations, the optical equipment which was used follows the IOTA/ES recommendation. It is based on a 100/1000 mm Maksutov-optic, a 535 nm filter and the IOTA/ES solar filter [2]. After reduction of TSE21082017 [4] the kind of camera used within the set-up and data format was changed: a 12-bit digital camera (FLIR Chameleon) was used to record a series of images in FITS format. The time protocol is done by time stamps in the FITS file by the recording software *FireCapture* [5]. The PC time is synchronized by GPS time via GPS receiver and NTP. Any differences PC-time minus GPS-time, are registered in time protocol. The accuracy of the time stamps, created by *FireCapture*, was tested in advance by a 1-PPS LED signal observed with the camera in video mode. The differences time stamp versus LED signal were never found to be more than 20 ms.

Following the station code syntax in [2], the station is named 2019CLN1. The northern station was located close to the small village Domeyko, near the Pan Americana highway. The observation place was 700m within the totality zone. At this place the predicted length of totality was 16 s. Position: Latitude 28° 57′ 37.5″ S; Longitude 70° 53′ 32.4″ W; h=770 m (WGS84-EGM96)

Figure 5. The zone of totality for TSE 02072019 in Chile. The location of station 2019CLN1 is marked by a red arrow. Map provided by [7]. Map data: Google Maps, © 2020 TerraMetrics

Figure 4. The author prepares station 2019CLN1 close to the small village Domeyko, near the Pan Americana highway. The observation place was 700m within the totality zone. More eclipse chasers wait for the eclipse in the background. (Elke Guhl)

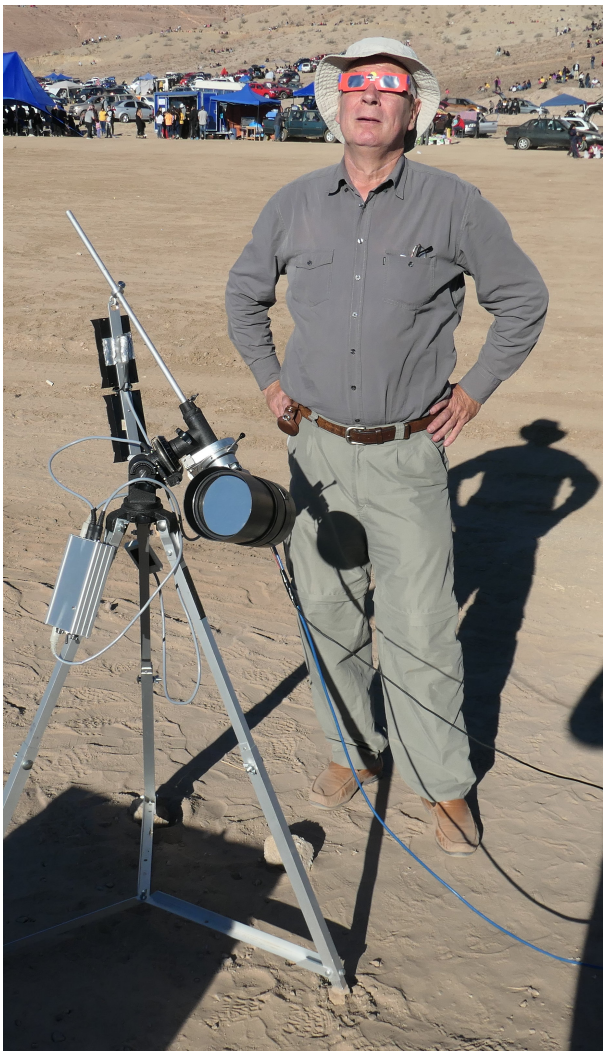

Figure 6. The author at his station is ready for the eclipse. The IOTA/ES-solar-filter is mounted on the 4-inch-Maksutov lens (Elke Guhl).

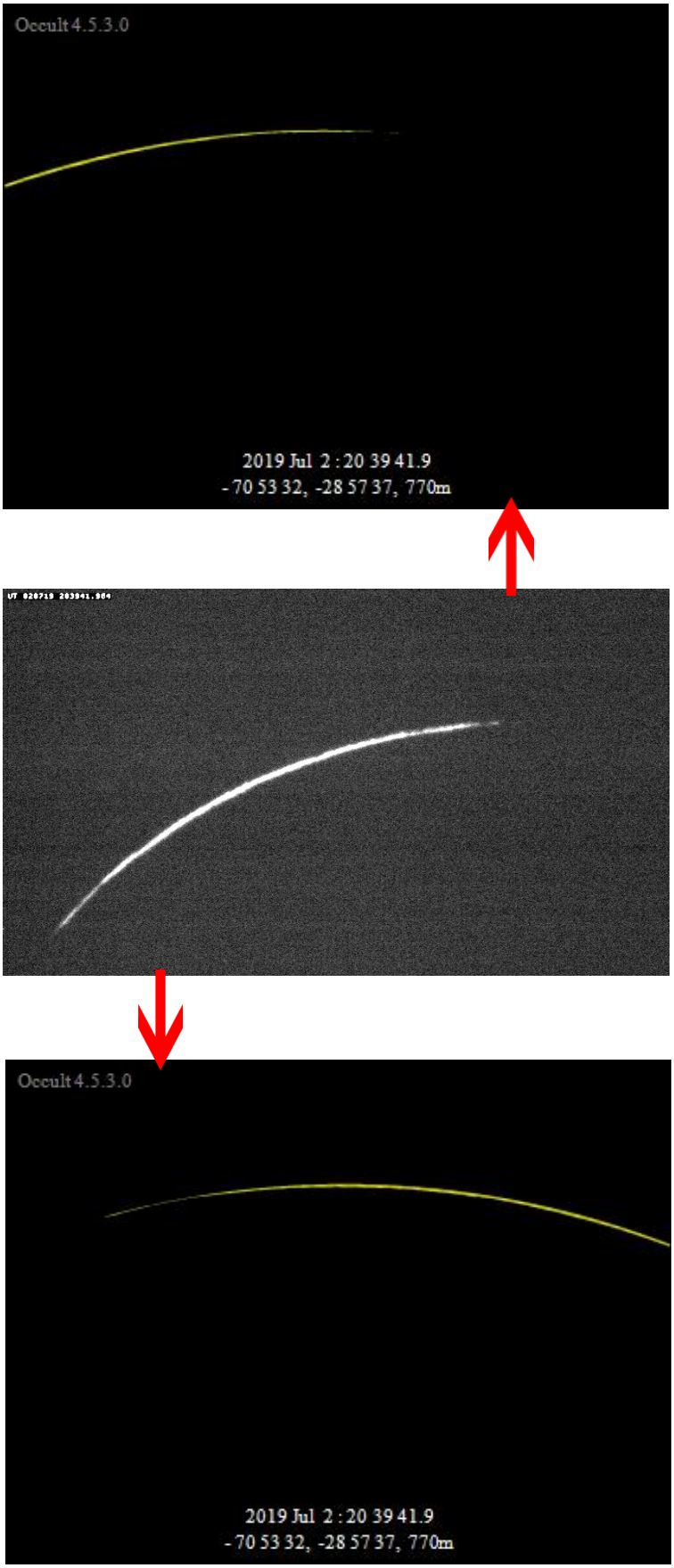

Figure 7 - 9 (top to bottom). Simulation and image at 20h39m41.9s, seconds before totality. The arc from the visible part of the sun reaches in the image from AA 7° to 54°. The simulation is split into two parts due to magnification. Figure 7 simulates the cups at AA 7°, figure 9 the cups at AA 54°.

Results

The FITS images have been visually analyzed by the author. The inspection was done twice on different monitors and on different days. Only those beads which could be visual easily identified were included in the analysis, which was performed like described in the method section (using LOLA limb data).
Table 1 contains the measurements from the northern station 2019CLN1 (observers Elke and Konrad Guhl), as well as the differences ΔR_s to the solar radius as derived from analysis described in the method section using *Occult*.

Station 2019CLN1 (Elke and Konrad Guhl)			
Time UTC	Axis Angle	Type	Difference ΔR_s to solar radius
20:39:45.2	54°	D	-0.04″
20:39:59.2	31.6°	D	-0.12″
20:40:02.4	21.7°	D	-0.03″
20:40:05.6	18.4°	D	-0.04″
20:40:11.2	11.4°	D	-0.04″
20:40:35.8	356.8°	R	-0.13″
20:40:36.0	347.8°	R	-0.01″
20:40:36.0	348.4°	R	-0.03″
20:40:36.8	343.2°	R	-0.22″
20:40:36.9	346.1°	R	-0.14″
20:40:38.1	352°	R	+0.13″
20:40:41.5	329.58°	R	-0.08″
20:40:42.1	331.9°	R	-0.30″

Table 1. Measurements (timings) of the observed Baily's Beads (D=Disappearance, R=Reappearance) and derived corrections to the solar radius.

From (unweighted) averaging of the data given in Table 1, a mean of ΔR_s = -0.08'' with a standard error of the mean (SE) of 0.03'' and a standard deviation (SD) of 0.10'' is derived. By multiplying the SE with the factor 1.96 we get approximately the SE at the 95% confidence level. Thus, we note ΔR_s = -0.08'' ± 0.06'' as our final result for the correction to the solar radius.

Discussion

The value adopted by the IAU General Assemblies in Beijing (2012) and Honolulu (2015) for the Astronomical Unit is 1 AU = 149,597,870,700 m exactly and for the nominal solar radius R^N_0 = 6.957 * 10^8 m. In arc seconds, the solar radius is now fixed at a value of 959.22″ (at unit distance).

For TSE02072019 we derived a value of ΔR_s = -0.08'' ± 0.06''. For comparison, previous results obtained by the author are given below:

2016: ΔR_s = -0.02″, derived for TSE01092016 [6]
2017: ΔR_s = +0.03″, derived for TSE21092017 [4]

The main uncertainty is the timing (detection) of the disappearance / reappearance of the beads. Table 2 shows the results of a reduction of 3 beads with premature / delayed registration of the D/R event by 0.1 s as an estimate for the assumed timing error. In this example a timing error of ±0.1 s propagates to a change of the radius correction ΔR_s of not more than 0.02''.

Beads at AA	t (s)	ΔR_s
31.5° too early	59.1	-0.14″
31.5° observation	59.2	-0.12″
31.5° too late	59.3	-0.10″
356.8° too early	35.7	-0.13″
356.8° observation	35.8	-0.13″
356.8° too late	35.9	-0.14″
331.9° too early	42.0	-0.31″
331.9° observation	42.1	-0.30″
331.9° too late	42.2	-0.30″

Table 2. Estimation of the error in ΔR_s caused by timing errors (here by applying +/- 0.1 s) for 3 beads.

Conclusion

The results of this Beads observation show a high variation within the data (the standard deviation with 0.10'' is larger than average). This can be interpreted as a hint towards low significance of this factor. It is suggested to try a different approach for estimating ΔR_s, beyond calculating an average of the values derived from the bunch of observed beads. For a further investigation of trends in the solar diameter, we propose an analysis of the same bead on multiple occasions (eclipses). A re-interpretation of previous observations is planned and shall be published here.

Acknowledgement

The author thanks M. Xavier Jubier for the fruitful e-mail discussion in the planning phase of the expedition and the helpful web page [7].

References

[1] Herald, D. Occult software
http://www.lunar-occultations.com/iota/occult4.htm
[2] Sigismondi, C. et. al. Baily's Beads Atlas in 2005 - 2008 Eclipses, Solar Physics, Volume 258, Issue 2, pp 191-202.
[3] Espenak, F., NASA, https://eclipse.gsfc.nasa.gov/eclipse.html
[4] Guhl, K., Tegtmeier, A. Baily's Beads Observations during the Total Solar Eclipse 2017 August 21, JOA 2018-03, pp. 19-21
[5] Edelmann, T. FireCapture software, http://www.firecapture.de/
[6] Guhl, K., Tegtmeier, A. Baily's Beads Observation during the annual eclipse 2016 Sept. 1, JOA 2016-04, pp. 15-18
[7] Jubier, X. „travel and eclipse site", http://xjubier.free.fr/

Further Reading

J. P. Rozelot et.al. "A brief history of the solar diameter meas urements -a critical quality assessment of the existing data" Proc. International conference on "Variability of the Sun and sun-like stars: from astroseismology to space weather", Baku, Azerbaijan, 6 - 8 July 2015

XZ 103822 - A New Double Star Detected by Lunar Occultation

Alex Pratt • IOTA/ES • BAA • Leeds • England • alex.pratt@bcs.org.uk

ABSTRACT: The author recorded a number of lunar occultations on the night of 2019 April 12, one of which, 10.3 V-mag XZ 103822, did not have an instantaneous disappearance. Analysis of its light curve shows it is a previously unreported double star with components of 10.7 mag and 11.5 mag, and a separation of ~0.2" at the time of observation.

Introduction

In their article in JOA 2020-01 [1], Dave Gault and Dave Herald explained that lunar LASER ranging, lunar satellite altimetry and *Gaia DR2* star positions now enable us to predict lunar occultations with great accuracy, but amateurs' observations of ordinary 'total' occultations are not redundant, they can be used to test the accuracy of their timing equipment.
Areas of occultation work where an observer can make a contribution are:

Grazing occultations - In JOA 2019-04, Wojciech Burzyński [2] discussed his excitement in recording grazing occultations and the value of his results, where he contributes to studies of the polar regions of the Moon.

Double stars – an occultation of a double star can produce a 'stepped' light curve, from which the magnitudes of its components can be derived. Observations from stations across a baseline of several hundred km are used to estimate the PA and separation of the component stars. Members of IOTA and its worldwide sections monitor known and suspected double stars, and they sometimes discover a new double star during an occultation.

Kepler2 stars – the light curve from a lunar occultation of a star monitored by the *Kepler Exoplanet K2* mission is of value, in case the star is a non-single system.

Traditionally, lunar occultation observers operate analogue video cameras in non-integrating mode, i.e. 25 frames per second (PAL system) or 29.97 fps (NTSC). If the signal to noise ratio is good the deinterlaced fields can be analysed, giving 50 fields per second (PAL) or 59.94 fields per second (NTSC). In Europe, Jan Mánek (IOTA/ES total occultations coordinator) has pioneered the use of digital imaging cameras, selecting a small Region of Interest and running at frame rates >100 fps [3].

The Occultation of XZ 103822

The evening of 2019 April 12 was clear at my back-garden observatory (MPC Z92), with a temperature of 1°C and a slight breeze. The First Quarter Moon was at a favourable altitude, the seeing was good, so *Occult's* [4] magnitude limit was increased to list predictions of stars to 10th mag. A 28cm aperture f/10 SCT equipped with an IR/UV filter and a Watec 910HX video camera operating at 1/50th second recorded several lunar occultations to a laptop computer using *VirtualDub* [5] and Lagarith Lossless Codec compression [6].
The 10.3 V-mag star XZ 103822 was predicted to disappear at the dark limb (DD) at 20:57:15.3 UT. Its disappearance wasn't instantaneous. The light curve was analysed at video frame level (25 fps) with *Limovie* [7] (at field level the light curve had a poor S/N ratio and was too noisy). The diffraction analysis gave a step duration of 0.423 seconds and, assuming a combined V-magnitude of 10.3, the component stars were estimated to be 10.7 mag and 11.5 mag. The radial velocity of the limb at the instant of occultation was 0.465"/sec, hence the separation of the component stars was >0.2". The PA at the limb was 110.9° [4].

Star XZ 103822 in Gemini

Coords. (J2000): RA 7h 40m 38.72s, Dec +20° 52' 50.11"
Colour index (B-V) +0.7

Derived double star data:
Mag. A 10.7 ± 0.1 (V)
Mag. B 11.5 ± 0.1 (V)
Epoch 2019.28
Separation > 0.2"
PA at epoch between 21° and 201°

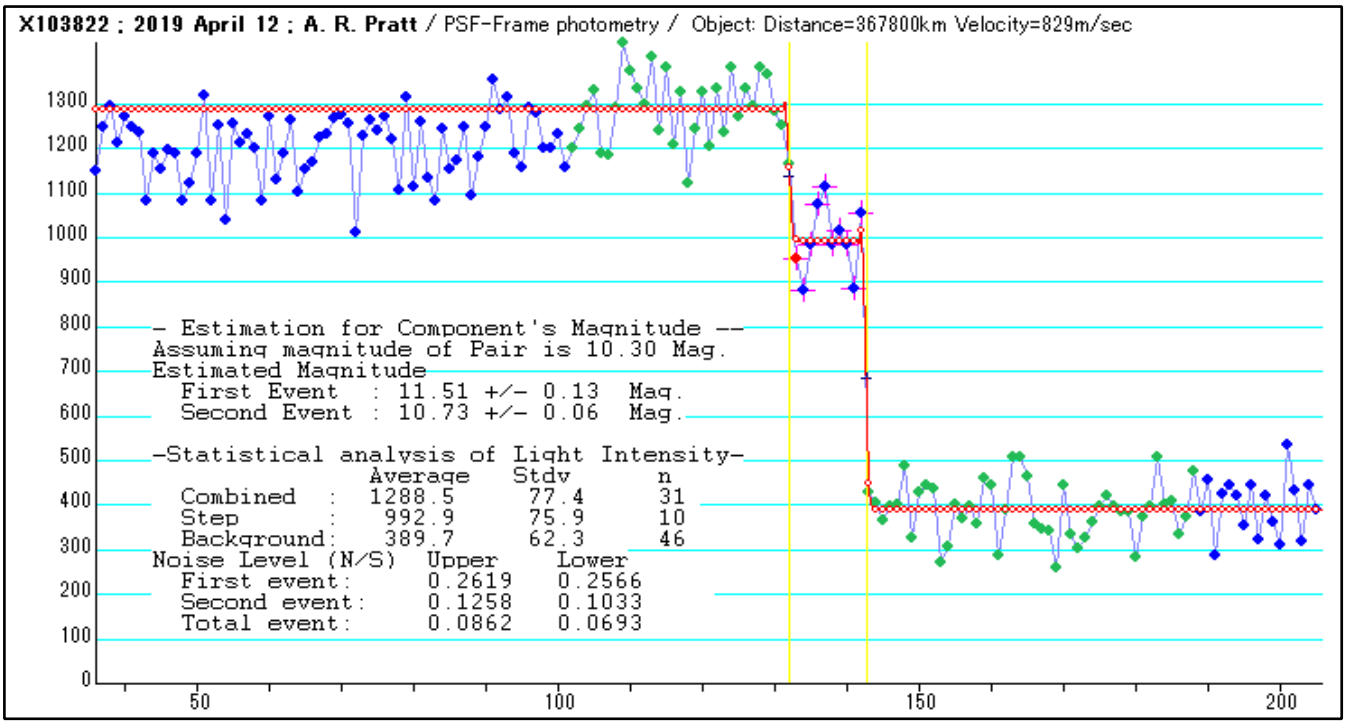

Figure 1. Limovie *diffraction analysis of the disappearance at the dark limb of XZ 103822 on 2019 April 12.*

Follow Up

A double star report was submitted to Brian Loader (IOTA double star coordinator)[1] and Tim Haymes (BAA occultations coordinator). Brian replied that it looked to be a discovery of a previously unknown double star and he hadn't received any other observations of XZ 103822 [8]. There are no observations of this star in *Occult's* Historical Occultations Archive and it is not listed as double in the *Washington Double Star Catalogue* or the *Interferometric Catalogue* [4]. We were coming to the end of its current series of occultations so it was likely to remain unconfirmed for several years. A short paper was submitted to the *Journal of Double Star Observations* [9] and the star's light curve is now in *Occult's* light curve dataset.

Summary

It will be interesting to see if *Gaia DR3* and/or *DR4* confirm the nature of XZ 103822 [10]. Whatever *Gaia* reveals, amateur astronomers can monitor this star when its lunar occultations resume in 2028 through to 2029, long after *Gaia* has ceased collecting data.

Observing lunar occultations of known and suspected double stars is an area in which the amateur can participate. In addition, a recording of the disappearance or reappearance of an 'ordinary' star could lead to the discovery of a double star. Not all is 'done and dusted' in the field of lunar occultations.

[1] Brian Loader (RASNZ,NZ) served as IOTA's double star coordinator for many years. In late 2019 he handed over the reins to Martin Unwin (NZ).

References

[1] Gault. D. & Herald. D., - All-Of-System Time Testing Using Lunar Occultations, Journal for Occultation Astronomy, No. 2020-01, Vol. 10 No. 1, pp. 9-13
[2] Burzyński. W., - The Chase for the Faintest Grazing Occultation – A Personal Report, Journal for Occultation Astronomy, No. 2019-04, Vol. 9 No. 4, pp. 3-8
[3] http://www.esop37.cz/sbor/L2-4_Manek_lecture.pdf
[4] http://www.lunar-occultations.com/iota/occult4.htm
[5] http://www.virtualdub.org/
[6] https://lags.leetcode.net/codec.html
[7] http://www.astro-limovie.info/limovie/limovie_en.html
[8] Loader, Brian, Personal communication (2019 April)
[9] http://www.jdso.org/volume15/number4/Pratt_528_529.pdf
[10] https://www.cosmos.esa.int/web/gaia/science-performance

Further Reading

White, N. M. Stellar Multiplicity Discovery By Lunar Occultations, Journal: Complementary Approaches to Double and Multiple Star Research, ASP Conference Series, Vol. 32, IAU Colloquium 135, 1992, H.A. McAlister and W.I. Hartkopf, Eds., p. 486.
Bibliographic Code: 1992ASPC...32..486W

Richichi, A., Fors, O., Cisano, F. and Ivanov, V. Final Binary Stars Results From The VLT Lunar Occultations Program, arXiv:1401.0656 [astro-ph.SR], (2014)

Using the Windows Clock with Network Time Protocol (NTP) for Occultation Timing

Hristo Pavlov • IOTA/ES • Reading • United Kingdom • hristo_dpavlov@yahoo.com
Dave Gault • WSAAG • Hawkesbury Heights • Australia • davegault@bigpond.com

ABSTRACT: Composite video has been used for many years to observe and time occultation events, mainly because Video Time Inserter devices can accurately time-stamp each video image just before it is recorded. The use of Personal Computer (PC) as a video recorder makes use of the *Microsoft (MS) Windows* clock to time-stamp video recordings. There is anecdotal evidence of this method being used with Internet NTP servers with a timing accuracy varying from a few milliseconds to a few seconds.

In this paper we demonstrate, based on 528 hours of 47.5 million continuous measurements, that a *Windows* system that uses the correct hardware and software, and a correct workflow, is capable of utilising the *Windows* Clock synchronised by Internet NTP servers to timestamp a video with an accuracy of better than 15 ms in 99% of the time.

We further provide guidance that will enable a much wider range of video equipment to be successfully used to time occultation events.

Introduction

Achieving a millisecond timing accuracy with analogue video has been well established with video time inserters such as IOTA-VTI [1] and others. When it comes to digital video cameras the timing options are a lot less established and the work is still ongoing. Commercial QHY174M-GPS cameras [2] and systems such as ADVS [3] and others [4, 5] are capable of achieving millisecond accuracy but they are either not widely available or are expensive for the amateur community. With the increasing availability of new digital cameras more observers are attempting to time video recordings using the computer clock synchronised using internet NTP servers and the vast majority of the observers are using the *Windows* OS. This raises the question of what timing accuracy is possible with this set-up.

The problem of accuracy is two-fold. Firstly, if the computer clock was perfectly synchronised then what would be the ability of the OS to read the clock accurately; and secondly how accurately the clock could be synchronised using NTP servers on the Internet with the hardware used by the OS.

The ability of the *Linux* OS to accurately read the system clock is well known and *Linux* servers are used worldwide in time-critical infrastructures. Early versions of *Windows*, including *Windows 7*, had various problems that could sometimes provide a clock resolution of only 16 ms, however with recent development *Windows 10* is now capable of providing microsecond resolution [6] via the GetSystemTimePreciseAsFileTime function [7]. While this brings *Windows* at par with *Linux* regarding timing precision it is a separate question of how accurate those timestamps can be. It has been shown that when the clock is accurately set *Windows 10* is capable of an accuracy close to a microsecond [8]. This claim however cannot be automatically made when the clock is synchronised from Internet NTP servers and the time is retrieved by an arbitrary software package. Our research focuses specifically on determining what accuracy is achievable in an environment where a below average internet ADSL connection is used to synchronise the system clock using Internet NTP servers.

In the Background section of the paper we first discuss the various known hardware and software requirements for a *Windows* system to be capable of keeping accurate time and also examine in detail the various aspects of achieving and claiming a timing accuracy on *Windows* using Internet NTP servers. We then put a compatible system to the test as described in the Experimental Setup section. We present our results and discuss them. We conclude by summarising the results and providing remarks for further studies and recommendations for software authors on how to enhance video recording to help achieve and claim a better *Windows* Clock timestamping accuracy.

Background

Hardware and Operating System Requirements

The problem of obtaining and asserting that *Windows* UTC timestamps of video frames are accurate is complex and the first very important steps towards this is to assess the ability of a particular *Windows* PC and OS to keep time accurately. It is important to note that while within this section we refer to *Windows* specifically, everything we discuss regarding hardware requirements is also valid for other operating systems, including *Linux*.

The operating system may either use a dedicated crystal oscillator

on the motherboard to provide periodic ticks or it may use the internal clock of the CPU core.

The use of crystal oscillators in electronics is well established [9]. The rate of oscillations is set during manufacture and a tolerance is specified, expressed in parts per million (ppm), called the maximum frequency offset. The frequency offset will allow a constant drift from the base frequency. The rate of oscillations is also affected by variations in operating temperature. Modern CPUs can have multiple cores and have power management features or Turbo Technology, all of which could affect the frequency of the CPU-core clock unpredictably, depending on workload.

The only way to guarantee that the retrieved *Windows* time will not be affected by multi-core and power management issues will be to make sure that the time is based on the crystal oscillator on the motherboard. This is possible only if the CPU has a feature called Invariant TSC and that this feature is supported by the *Windows* OS.

The invariant TSC will run at a constant rate in all ACPI P-, C-. and T-states. The invariant TSC is based on the invariant timekeeping hardware (called Always Running Timer or ART), that runs at the core crystal clock frequency. TSC reads are much more efficient and do not incur the overhead associated with a ring transition or access to a platform resource [10].

The above shows that in today's computers for time to be kept accurately by the OS it is necessary that your CPU (hardware) supports the Invariant TSC feature and your operating system is able to take advantage of this feature.

- The majority of *Windows 7*s support Invariant TSC
- *Windows 8.1* is capable of using the Invariant TSC
- *Windows 10* is capable of using the Invariant TSC and is recommended because of the additional improvements made to the *Windows 10* kernel and task scheduler [11].

While most modern PCs should support the Invariant TSC feature, we provide a small utility, called *OccuTimeCheck* [12] to help you check this. Additional information on the timekeeping accuracy of *Windows 10* with Invariant TSC is available online [6, 8].

Setting the System Clock via NTP

For Internet NTP synchronisation to work well very fast internet connection is required - ideally ADSL2+ or better. NTP synchronisation algorithm assumes that the client-server, request-response time is symmetrical. However in practise the propagation delay is asymmetrical due to the difference in upload and download bandwidth typical in all end user commercial providers. The more expensive DSL internet connections guarantee symmetrical propagation, but end users typically use the asymmetrical ADSL, where the A stands for asymmetrical. In order to minimize the error from the asymmetrical request-response, it is very important to choose NTP servers that are close to your physical location.

The NTP delay is assumed to be half the round trip (ping) time to the server. Based on this a good rule of thumb to estimate the maximum error of the NTP synchronisation due to the asymmetrical nature of the request-response propagation will be half of the latency to the used NTP server. A latency of 50 ms will mean a maximum error of 25 ms. Typically, the actual error from the asymmetrical connection will be much smaller than this.

Most countries and regions operate an NTP server pool or virtual cluster of time-servers. An online search will quickly find some appropriate server addresses that are close to your physical location. Most reliable NTP software utilises an NTP server pool and monitors the pool for delay, offset, and jitter and ranks the servers in the pool, using the best for synchronisation.
The NTP clock synchronisation software could use different methods to adjust the system clock and the choice of methods will have an impact on how well the software will be able to do its job. The SetSystemTime [13] function is used to make the clock jump forwards and backwards without changing the base frequency while the SetSystemTimeAdjustment [14] function is used to correct the base frequency so the time doesn't go backwards and the drifts from UTC are corrected smoothly.

NTPv4 offers a more comprehensive method of clock synchronisation defined in RFC-5905 [15]. The NTPv4 algorithm uses a combination of the two functions above to achieve and maintain the correct time. It also uses a series of thresholds [16] with the goal of making adjustments as smooth as possible.

Acquisition Delay

Even if we have a perfect time reference at the time when a video frame is handled by the recording software, there is the valid question of how we know, based on this time, when the optical exposure actually occurred. This is where Acquisition Delay comes into play. Figure 1 shows the total delay encountered in various parts of the system with letter-assigned segments to help in the discussion.
The optical exposure happens in the **A** segment inside the camera. Once the exposure has finished the chip will have to be read out and the image prepared for transmission. This is represented with the **B** segment which will depend on the camera firmware and is expected to vary between camera models and between different firmware versions of the same camera. The image will then be sent to the PC over a cable and this is represented with the **C** segment. This time delay may depend on the type of port used (USB2, USB3, FireWire, Analogue etc) and on the cable itself.
On the PC side there will also be a hardware component receiving the signal. This could be for example an analogue or FireWire PCI or USB frame grabber or it could be the USB port on the motherboard. The delay introduced by this component is shown with **D** and is expected to be hardware dependent i.e. changing the frame grabber or the physical USB port used could change

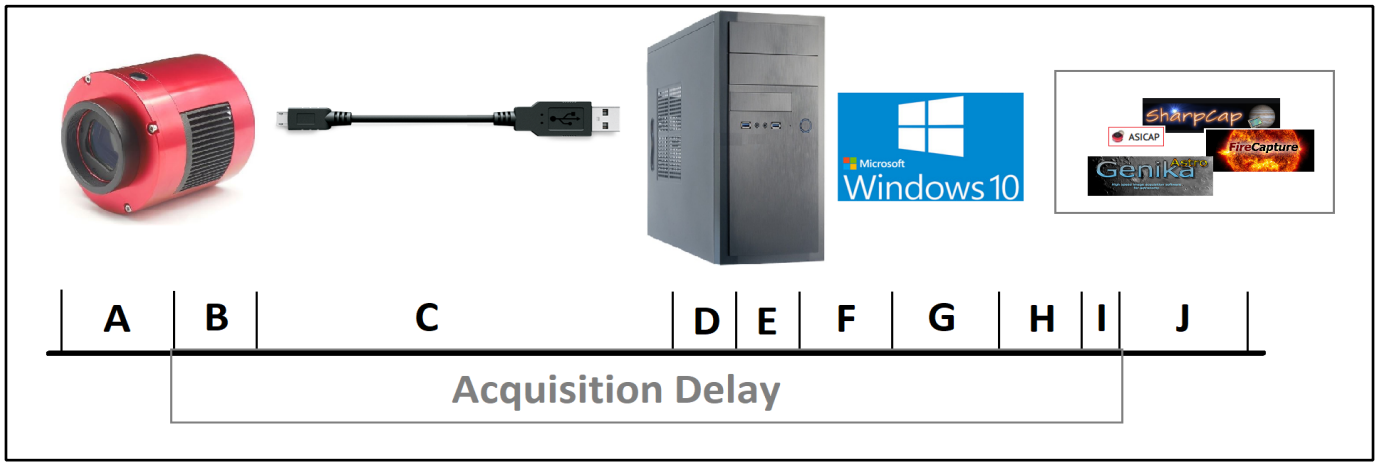

Figure 1. Time delays in a video acquisition system using a PC. The size of the named segments does not correspond to the actual size of the experienced delay in the corresponding named segment.

this part of the delay. It is possible that this hardware component also has its own firmware and a corresponding logic. The delay introduced by the firmware of the grabber is shown as **E**. Before *Windows* can receive the image it requires a software driver for the component, either a USB driver or a frame grabber driver, to process the image which will take some time. This delay is the **F** segment and will depend on the driver and its version. Some digital camera vendors provide the driver and different versions of the driver could have different delays. Once the image is received by the *Windows* core (also known as ring 0) there will be possible interrupts involved before the image is passed on. This delay is represented with the **G** segment and it could vary with major operating system updates. Now the image is almost ready to be passed on to the recording software, however this needs to happen on a particular software thread. Based on the OS task scheduler there will be a delay represented with the **H** segment and this delay could also vary with major operating system updates. Now the image has been given to the recording software, however each software will handle it differently and there could be some time involved before a timestamp is associated with the received image. This delay is represented with the **I** segment. Ideally the *Windows* Clock timestamp will be assigned as soon as possible but after **I** we should have a timestamp. The **I** delay will depend on the recording software used and could vary with major software updates of the recording software. Now the frame is ready to be recorded into a file which will happen at some later time represented by the **J** segment delay. At last we have our image saved onto the computer.

The sum of the delays introduced from segment **B** to **I** (inclusive) is what we call Acquisition Delay. Some recording software may not assign an end of the exposure timestamp at the time the image was received, but could try to manipulate this timestamp using the exposure and the Acquisition Delay (if known) to derive a timestamp corresponding to the beginning or the mid-time of the exposure including or excluding the Acquisition Delay. In order to interpret the timestamp correctly and to apply the Acquisition Delay correction correctly it is very important to know what is the behaviour of the recording software which uses *Windows* Clock timestamps. It may be even possible to use some recording software to allow for configuring an Acquisition Delay and to be able to calculate the actual optical timestamp.

It is reasonable to expect that if we don't change any of the hardware, firmware and software components of a system, the Acquisition Delay will be constant with some random jitter that may be expected to have a normal distribution. The only way to measure what the Acquisition Delay is would be to take multiple measurements where the optical exposure timestamp is known and to compute the median observed delay. This is part of what we did in our experiments presented below.

Experimental Setup

The testing was performed on a Toshiba Qosmio laptop with an Intel i7 Processor and 8Gb RAM. The Operating System was *Windows 10.0.18363.720*. For the majority of the tests, the PC used a Wi-Fi connection to the home router. We also present some test results where the test PC was connected to the router via a CAT5 LAN cable.

The internet connection was ADSL2 with a performance of:

- Wi-Fi - 2.3 Mbps download, 0.6 Mbps upload
- Cable - 3.9 Mbps download, 0.6 Mbps upload

A WAT-902 analogue non-integrating video camera was connected to an IOTA-VTI that maintained a fix on the GNSS[1] constellation and was used to time-stamp the video stream supplied by the camera. The time-stamped video stream was grabbed using a Startech SVID2USD device over a USB2.0 port.

[1] GNSS stands for Global Navigation Satellite System, and is the standard generic term for satellite navigation systems that provide autonomous geospatial positioning and atomic clock time with global coverage. Common GNSS Systems are GPS, GLONASS, Galileo, Beidou and other regional systems.

The *OccuRec* software [17] was installed and ran on the test PC. In order to minimize the size of the resulting files *OccuRec* was used in a special recording mode where it only recorded metadata for each frame but not the video frame image itself.

The following times were saved in the frame metadata:

- The UTC time reference at exposure time as obtained from the IOTA-VTI display using Optical Character Recognition (OCR) on the fly.
- The *Windows* clock timestamp at the time the frame was received by *OccuRec* using the function, GetSystemTimePreciseAsFileTime().

OccuRec monitored for dropped or duplicated frames and could occasionally record a debug video frame when it identified a problem with the frame order or was unable to OCR and verify the timestamp from the IOTA-VTI for a particular frame. *OccuRec* also maintained its own NTP server pool and recorded an NTP timestamp with each frame as well as the ping times to the NTP servers once per minute. One recording session lasted for at least 48 hours duration and the recorded .aav files were partitioned in a 24 hour series. *OccuRec* also recorded once per second information about the load of the system including CPU and Hard Disk utilisation as well as the available free memory (RAM).
The apparatus, software and time-sources were arranged as shown in Figure 2.

We tested 4 different methods to set the PC clock:

- The default *Windows Time* clock synchronisation mechanism of *Windows 10*, using time.windows.com
- *Dimension4* [18], ver.5.31, using ntp2.tpg.com.au as an NTP server with a median latency of 28.3 ms.
- *NetTime* [19], ver.3.14, using 0.nettime.pool.ntp.org and local servers including ntp2.tpg.com.au with a median latency of 26.7 ms
- *Meinberg NTP* [20], ver. 4.2.8p13-win32. The *Meinberg NTP* Server Monitor ver. 1.04 application was also used to record statistics for some of the sessions, including delays and currently used peer.

Tangra [21] was used to combine all the metadata recorded in each session and examine the difference between the IOTA-VTI provided UTC reference time and the *Windows* Clock time recorded when the frame was received. It is expected that the difference between those two times in the ideal case would be the constant Acquisition Delay i.e. the time needed for the video frame to propagate from the video camera to the recording video software.

Results

We present below the results for the four tested synchronisation methods with graphs for periods of 48 consecutive hours. On the graphs we define Delta Time as the difference between the *Windows* derived time for a single video frame and the corresponding UTC timestamp derived from the IOTA-VTI. We only show a small portion of all the graphs with the remaining ones made available online [22]. The entire 20GB of collected raw data, as well as a smaller 1.5GB Delta-Time-only data set, can be made available to interested researchers upon request.

Windows Time

Figure 3 shows that *Windows Time* was letting the clock drift 400 ms away from the reference before kicking in and adjusting it back quickly but gradually. The second day also showed a somewhat smoother adjustment but again it was letting the clock drift 400 ms. The *Windows Time* synchronisation mechanism was off by 100 ms to 450 ms for the entire 48 hour time period.

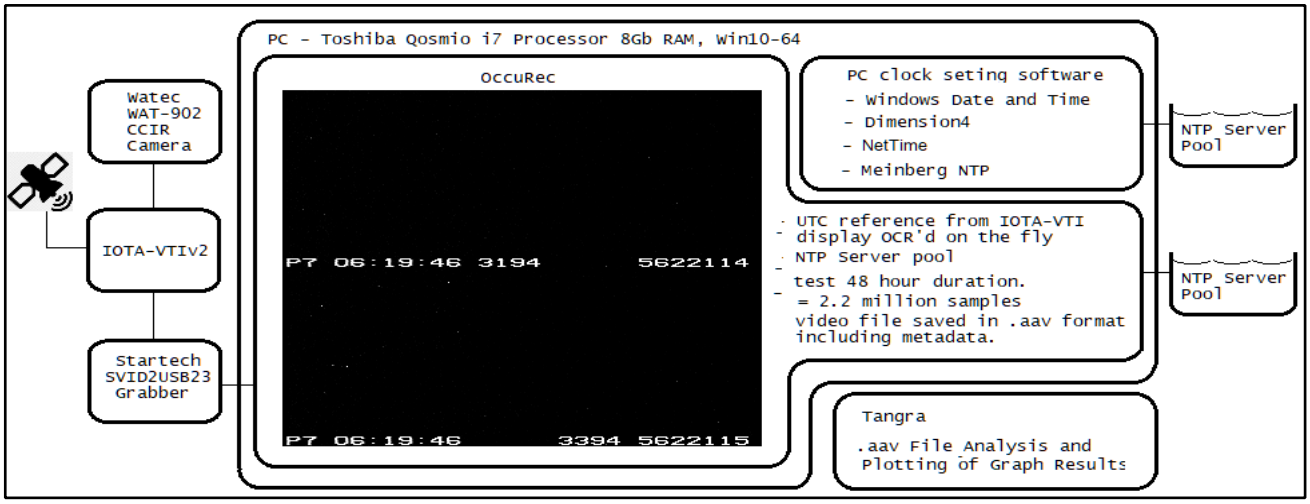

Figure 2. Arrangement of test apparatus, software and time-sources.

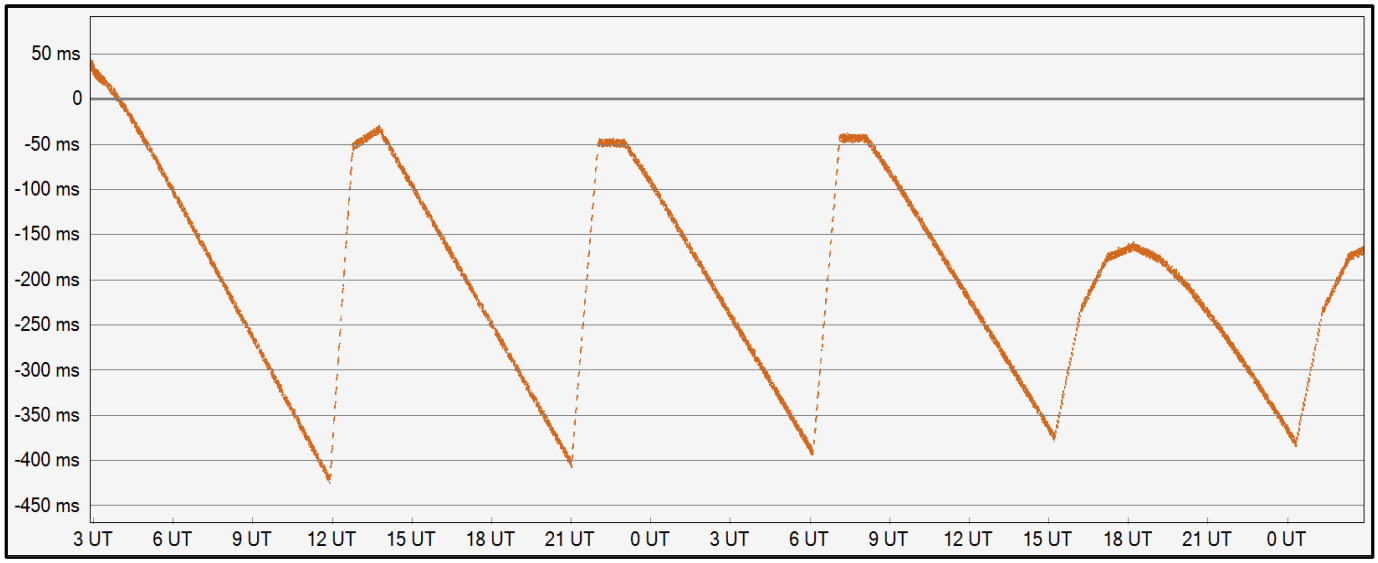

Figure 3. Delta Time of 4.3 million data points between 17-Jan-2020, 02:52 UT and 19-Jan-2020, 02:52 UT when the Windows clock was synchronised using the default Windows Time mechanism of Windows 10.

Dimension4

The second synchronisation tool we tested was *Dimension4*.

We obtained a total of 96 hours of data between 8 and 12 Nov 2019 and the Delta Time plot for two of those days is shown in Figure 4.

It is evident from the plot that *Dimension4* was setting the clock once every 10 minutes and was then letting it drift for 10 minutes until setting the time again.

The median value across the whole testing interval was +25 ms, which was only 25 ms off from true UTC. Surprisingly however the jitter was large and offsets of 300 ms and even 600 ms from UTC were observed in many 10 minute periods. While the main problem of the *Windows Time* method was that it was allowing the clock to drift too far away and for too long, the main issue with *Dimension4* was that while it was setting the clock every 10 minutes the error of each setting of the clock was bigger in many of the cases. The data obtained with *Dimension4* shows that in 95% of the time the accuracy was within +/- 220 ms from UTC.

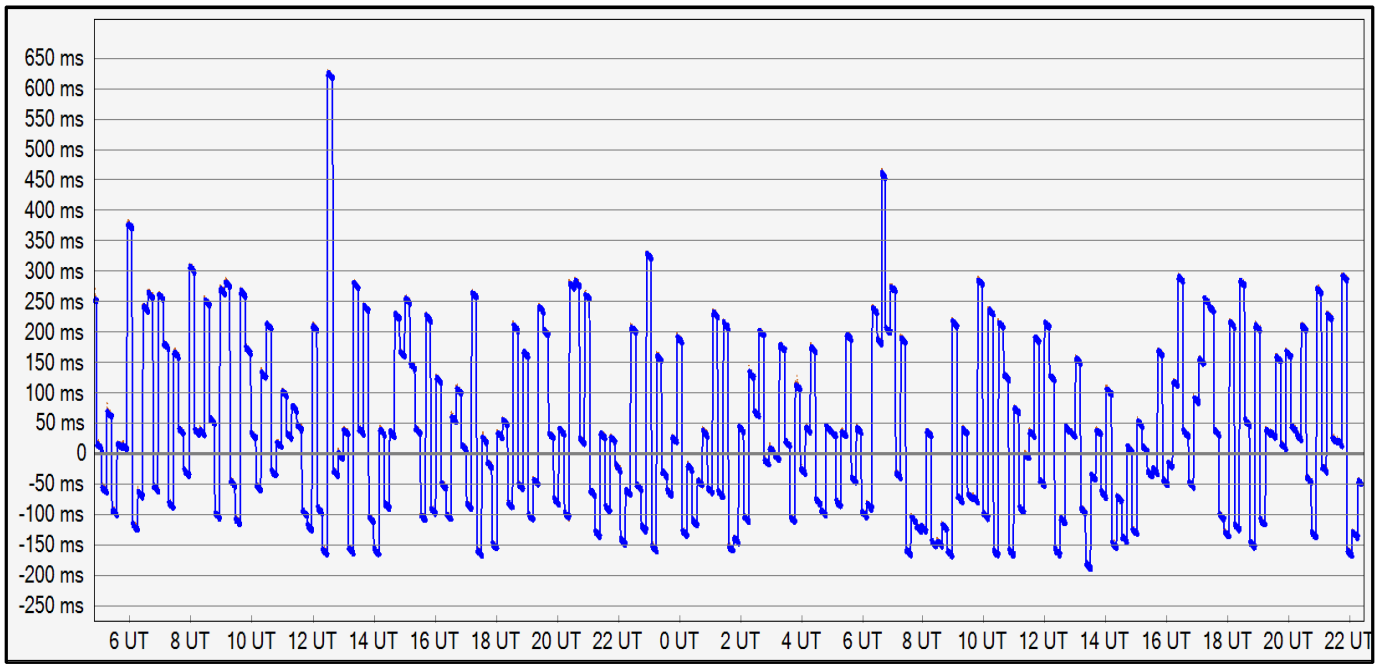

Figure 4. Delta Time of 3.7 million data points between 08-Nov-2019, 04:50 UT and 09-Nov-2019, 22:23 UT when the Windows clock was synchronised using Dimension4.

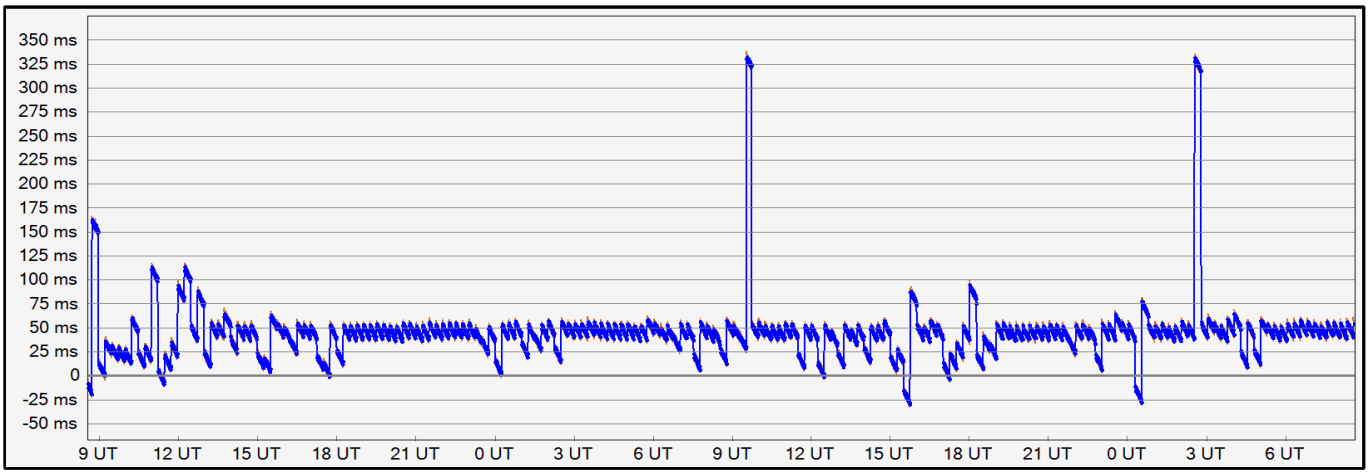

Figure 5. Delta Time of 4.3 million data points between 16-Mar-2020, 08:34 UT and 18-Mar-2020, 08:34 UT when the Windows clock was synchronised using NetTime.

NetTime

The third synchronisation tool we tested was *NetTime*. We obtained 48 hours of data presented in Figure 5. *NetTime* was doing small corrections of the drift every 2 minutes and larger corrections every 15 minutes. Over 70% of the time the *Windows* clock was within 10 ms of UTC however the remaining 30% showed occasional large offsets and for about 3 hours the *Windows* clock was more than 50 ms away, including being more than 300 ms away for 30 min. In 95% of the time the accuracy was within +/- 50 ms from UTC.

Meinberg NTP

The last tool we tested was the *Meinberg NTP* client. We obtained data for a total of 22 days (528 hours) which resulted in 47.5 million individual data points. *Meinberg NTP* demonstrated an ability to keep the *Windows* Clock synchronised with the highest accuracy from all 4 methods we tried. The clock was kept in sync mostly to within 10-15 ms from UTC except for two types of situations.

The first one was random unexpected shifts of usually 20-30 ms continuing for 1-2 hours with the largest one observed being a single shift of 80 ms away from UTC for 2 hours. Typically the fast shift was followed by a slow adjustment to get back to the correct time.

The second, and more significant source of larger offsets, was observed after a cold start of the PC where the errors were typically larger (30-80 ms) and it took 2-3 hours for the clock to settle to the +/- 10 ms interval. In one instance we observed a 300 ms offset immediately after a restart but it only continued in the first 10 minutes. Also in one instance it took 6 hours for the offset to come down from 80 ms to 10 ms from UTC.

For *Meinberg NTP* we show 4 graphs that demonstrate different aspects of what we observed. On the presented graphs the orange parts are the individual data points and the blue line is a 10-min median.

In Figure 6 we show the smoothly kept time by Meinberg with a small variation of +/-10 ms for the vast majority of the time.

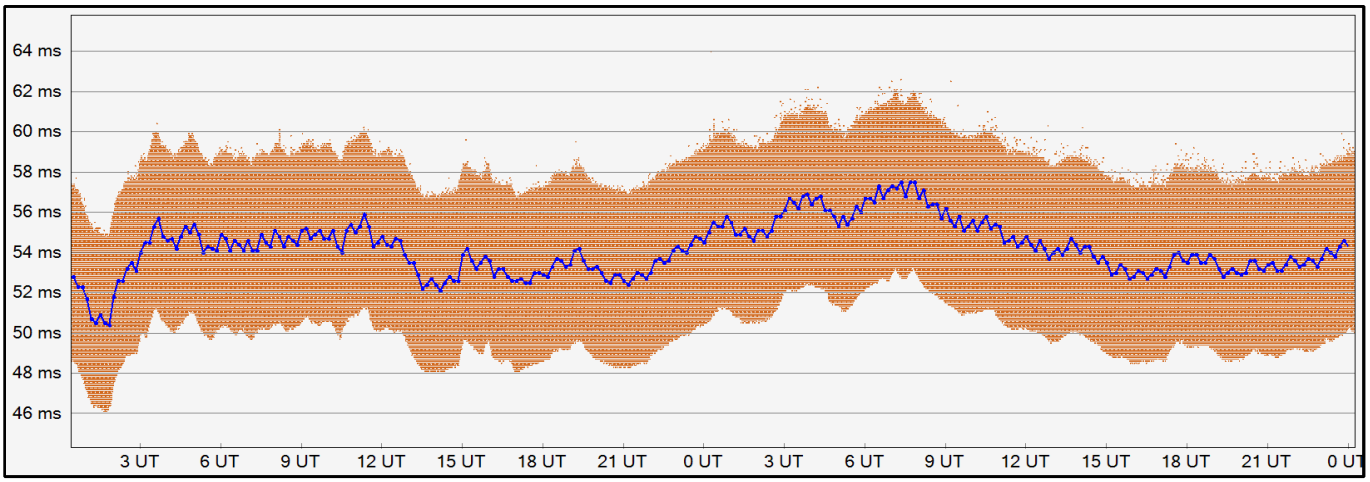

Figure. 6: Delta Time of 4.3 million data points between 08-Dec-2019, 00:25 UT and 10-Dec-2019, 00:15 UT, with a PC restart at the start.The graph excludes the first 10 minutes of the session where delta was at 300 ms.

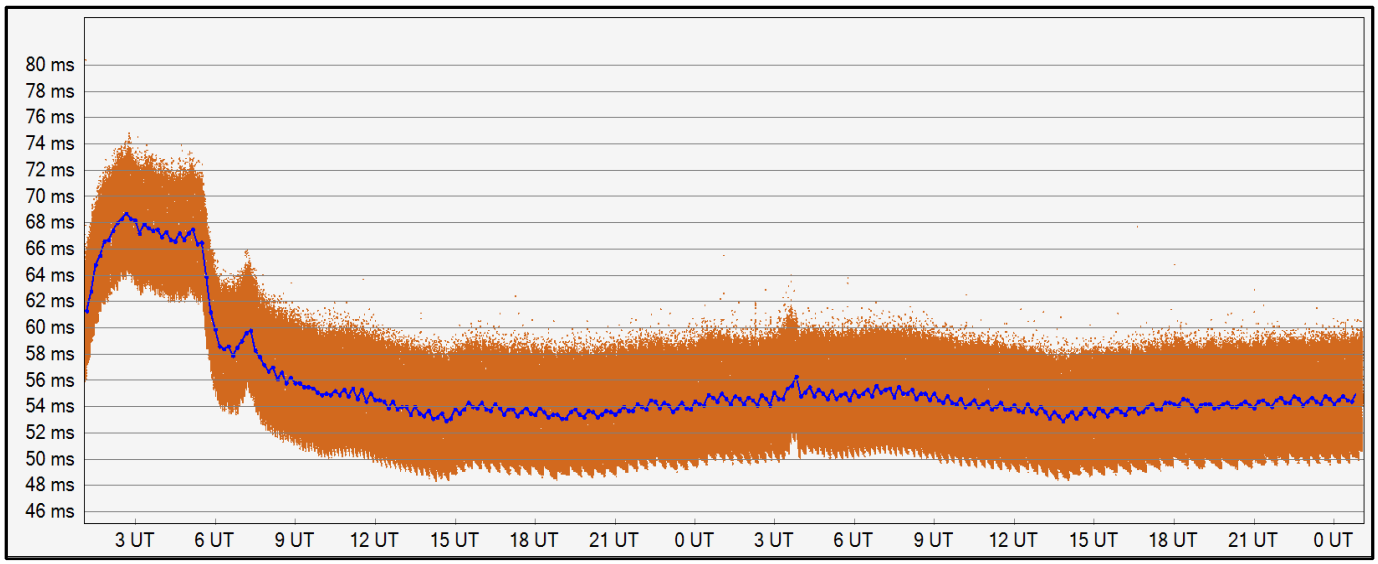

Figure 7. Delta Time of 4.3 million data points between 12-Nov-2019, 01:04 UT and 14-Nov-2019, 01:04 UT

In Figure 7 we show the initial variation after a cold-start - the clock in this instance drifted 20 ms from UTC and then slowly came back to the true time for within the first 2 to 3 hours. This behaviour was observed in 30% of the cases after a cold-start and drifts of up to 300 ms were observed. In the remaining instances of PC restarts this initial drift was smaller than 20 ms.

In Figure 8 we show an unexplained spike of approximately three hours duration. This occurred between 1 am and 4 am on a weekday morning when house-hold internet activity was minimal. The most likely explanation was delays in the internet network or an erroneous time reported by the currently used NTP server. We also run four days of testing using *Meinberg NTP* over a LAN connection including two PC restarts. The results matched those obtained from the Wi-Fi tests. We observed on both days, where the PC was restarted, the initial drift while getting the clock to a stable offset. The first day showed a larger initial drift starting from 80 ms from median and a more stable curve after the clock adjustment settled. The Delta Time plot from the last two days is shown on Figure 9.

Generally Meinberg was able to keep the *Windows* Clock in sync very well and for the entire data set it was +/-10 ms from UT in 97.9% of the cases and +/-5 ms in the 91.4% of the cases.

During the Meinberg testing we also deliberately added load to the system on a couple of occasions. The system was used to copy large files via USB and occasionally the disk activity was above 90%. The CPU activity during the entire testing interval was below 40%. There were no observed anomalies resulting from higher system load introduced by this system load test.

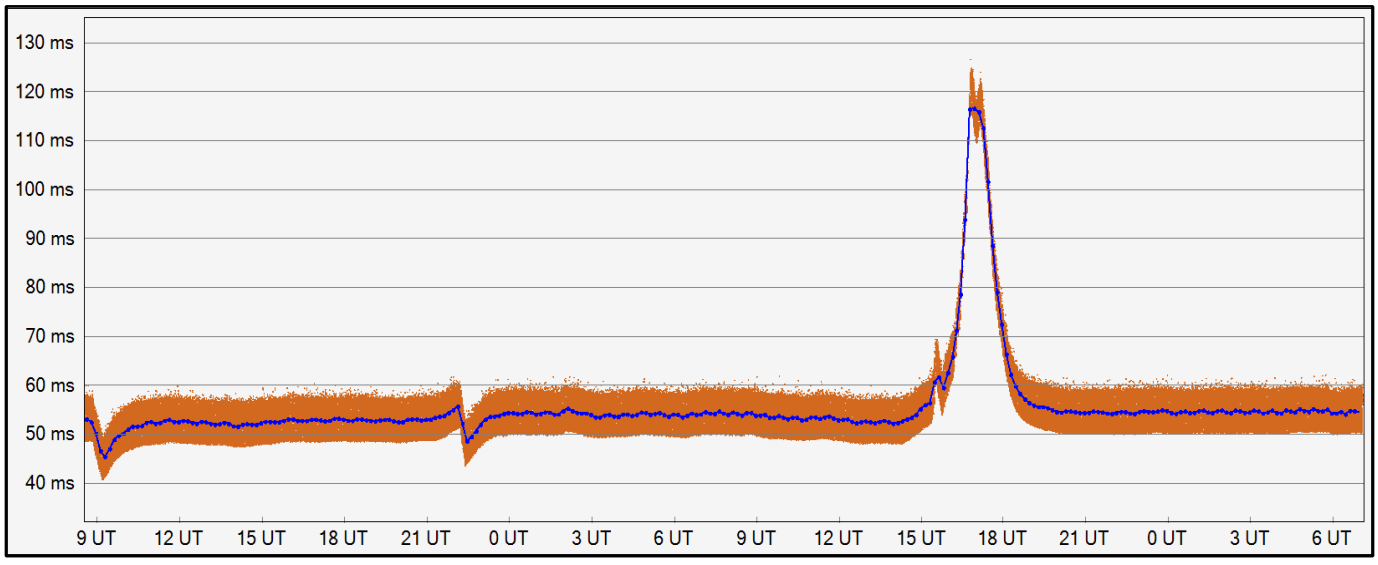

Figure 8. Delta Time of 4.2 million data points between 26-Nov-2019, 08:32 UT and 28-Nov-2019, 07:05 UT.

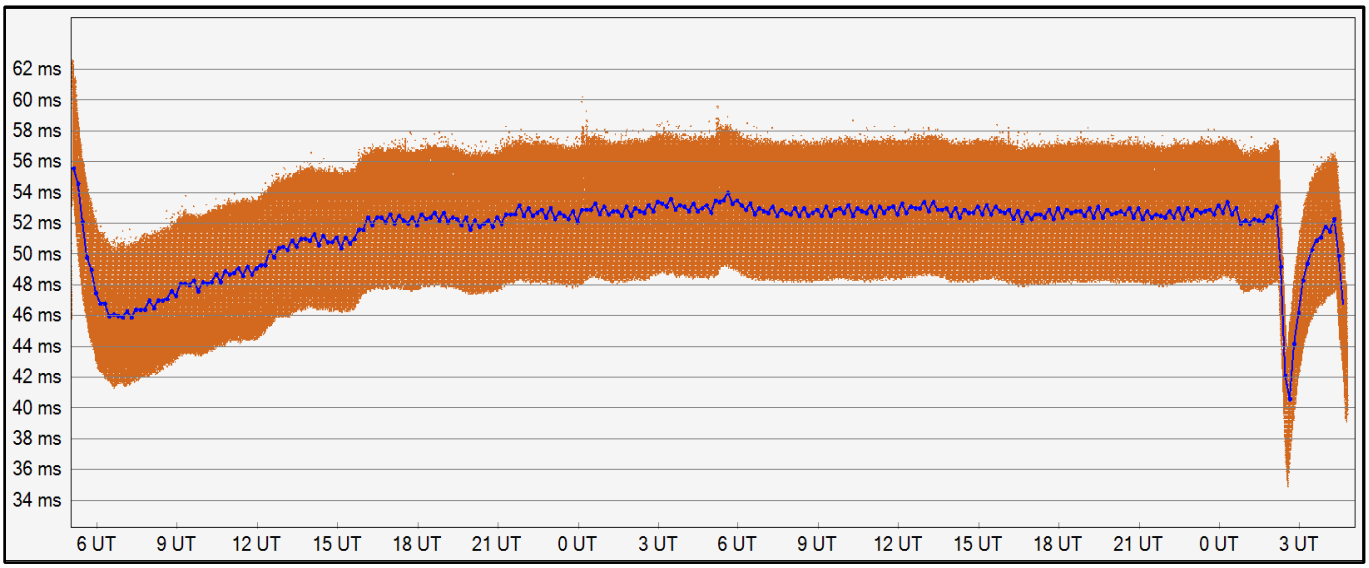

Figure 9. Delta Time of 4.3 million data points between 24-Mar-2020, 04:46 UT and 26-Mar-2020, 04:47 UT.

Discussion

The bad performance of the standard *Windows Time* synchronisation was not a surprise and the result we observed matched *Microsoft's* own claim of 1 sec accuracy of *Windows Time* [23].

It is interesting to note however the different types of observed system clock corrections. As neither *Dimension4* nor *NetTime* are NTPv4 clients all adjustments made by those two methods were not smooth and had a characteristic of a jump. In contrast the *Meinberg NTP* corrections had a very smooth nature but also showed longer times to recover from an occasional erroneous offset. All this is consistent with the expected behaviours of SNTP [24] and NTPv4 clients [16].

When it comes to LAN versus Wi-Fi, on the LAN plot for *Meinberg NTP* we see minor initial variations in the order of extra 2-5 milliseconds which were also observed during all Wi-Fi tests. The initial variations however eventually settled and for a period of 18 hours almost no variations were observed. From the total of 72 hours of LAN data we see that the LAN tests showed smaller overall variations after reaching the stable offset .This is consistent with a previous measurement comparing LAN with Wi-Fi [25].

An interesting question was what would be the distribution of the population of measurements of the very large dataset for *Meinberg NTP*. We show this distribution in Figure 10 in the Summary section.

The distribution doesn't appear to be normal and the likely explanation for this is that the errors are not exactly random but are dominated by the errors from the slow clock adjustments which are not expected to show a normal distribution. Nevertheless the distribution is largely symmetrical with a very small skew to the right. Because the distribution is not normal and because our dataset is very large, we chose to derive the *Windows* Clock accuracy directly from our single large dataset using symmetrical limits in an estimated confidence interval.

The Acquisition Delay, considered to be the true offset from UTC, was measured as the median of the *Meinberg NTP* dataset. It was determined to be exactly 54.2 ms within 99.9% confidence interval. We also cross-checked this value against the Acquisition Delay determined when the *Windows* Clock was synchronized using a local GNSS receiver.

In Table 1 we show a comparison of the Acquisition Delays determined when the different methods of *Windows* Clock synchronisation were used. This is also an interesting statistic that allows us to probe the different synchronisation methods for a potential bias. The medians are compared against the Acquisition Delay determined when the *Windows* Clock was synchronised using a device with a local GNSS receiver.

Synchronisation Method	Acquisition Delay
Dimension4	23.7 ms
NetTime	44.6 ms
Meinberg NTP	54.2 ms
Local GNSS	52.8 ms

Table 1: The Acquisition Delay as it would have been determined if the various NTP clock synchronisation methods were employed. They are compared against the Acquisition Delay as determined when the Windows Clock was synchronised using a local GNSS receiver.

From the comparison it is evident that the Acquisition Delays determined when *Meinberg NTP* and local GNSS were used differ only by 1.4 ms. This demonstrates that *Meinberg NTP* was able to synchronize the clock quite accurately. At the same time we also see that *NetTime* and *Dimension4* show a bias of 8.2 ms and 29.1 ms respectively. These values are well within the determined accuracy of those methods (see Table 2).

The biggest issue with *Meinberg NTP* seems to be the long time that was required after a cold start to get the clock from sometimes a large initial offset to the correct and stable time. This behaviour is however consistent with the algorithms defined in the NTPv4 protocol [15]. We suggest that the occasional large initial offsets are a result of the not very fast internet connection that was used by our test system and if the connection was much faster and the servers in the pool closer, large initial offsets would not have been observed.

Summary

Modern hardware using CPUs with an Invariant TSC feature together with the latest version of *Windows 10* allow for a greatly improved timing accuracy and for *Windows* machines to be used for timestamping video occultation recordings.

We tested four time synchronisation methods for setting the *Windows* Clock from Internet NTP servers over a 2.3 Mbps download and 0.6 Mbps upload ADSL connection. The observed timing accuracy using symmetrical limits with an estimated confidence interval of 99% for each of the methods is shown in Table 2. We use a 99% confidence interval because this provides a more realistic estimate in the environment an Internet NTP is operating, which can be affected by sudden network traffic congestion. The provided values have the meaning that in 99% of the time the accuracy will be better than the given value i.e. the value is the maximum expected error in 99% of the time.

Synchronisation Method	Accuracy
Windows Time	1 s [2]
Dimension4	320 ms
NetTime	260 ms
Meinberg NTP (less than 1 hour after a cold start)	240 ms
Meinberg NTP (more than 1 hour after a cold start	12.3 ms

Table 2. The determined accuracy of Windows Clock timestamps when the clock was synchronised by each of the tested methods on a Windows 10 system using a CPU with Invariant TSC.

A more granular distribution of the measured accuracy for *Meinberg NTP* is further shown in Figure 10.

Older versions of *Windows* and CPUs that do not support Invariant TSC may not be capable of achieving this accuracy.

During the testing the system utilisation was 40% or lower CPU load and under 80% of Hard-disk. Copying large files via USB put the Hard-disk usage to above 90% but this didn't result in a degradation of the timing accuracy of the video recorded at the same time.

Each individual video recording system will have its own Acquisition Delay and the derived timestamps will need to be corrected for it. Each observer should determine the Acquisition Delay of their own system. When the observer does not have access to a GNSS

[2] Based on Microsoft's own claim the default timing accuracy of the Windows Timer service achievable through standard internet NTP servers is 1 sec [23] so this is the value that we have adopted for Windows Time.

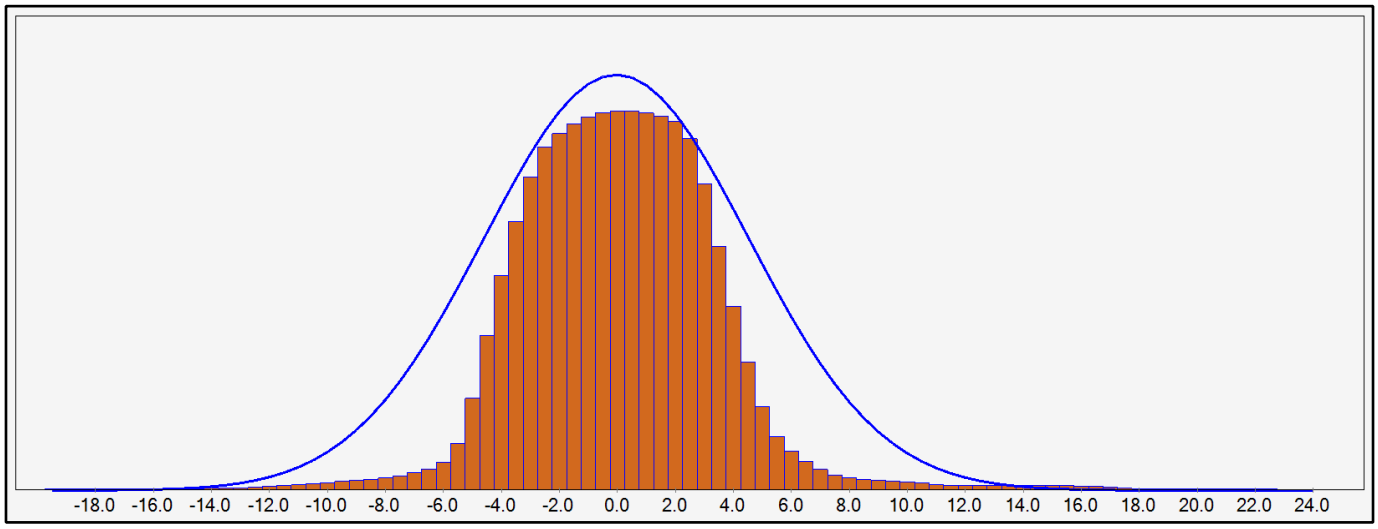

Figure 10. Distribution of the measured timing accuracy (in milliseconds) from all data points obtained with Meinberg NTP Windows Clock synchronisation. A best-fit normal distribution Gaussian is also plotted in blue. Outliers bigger than 25 ms have been removed from the graph and the fitting.

time reference to determine the Acquisition Delay of their system, the observation of lunar occultations may provide a means [26]. In our test system the observed Acquisition Delay was 54.2 ms. The accuracy figures shown in Table 2 assume that the Acquisition Delay is known and the timestamps have already been corrected for it.

To achieve maximum accuracy with *Meinberg NTP* we recommend the system to have been left running for at least 2 hours after the last cold start. More tests are recommended to understand how the accuracy can be improved when the system has been running for less than 2 hours after a cold start.

Further studies are also recommended with more accurate synchronisation methods based on local GNSS receivers, including for example local Raspberry Pi Stratum-1 NTP servers [27]. Also studies with high frame rate video cameras are required to better understand the effects of the high frame rate and USB traffic on the timing accuracy.

We further make the following recommendations to software authors of video recording software:

When NTPv4 is used the system clock is adjusted slowly and it may take a few hours from a cold start until the clock reaches a good accuracy. To provide higher confidence in any timestamps based on the system clock a video recording software can also record the system up time since the last cold start as metadata. This can be used during data reduction to determine what should be the expected error interval for the timestamp. The recording software can also record the model of the video camera so it is possible to determine if this camera can hold a constant frame rate.

Applying Acquisition Delay corrections is essential for achieving milliseconds accuracy. Recording software vendors should make it very clear when a timestamp has been associated with a video frame and if any corrections have been applied, such as subtracting exposure duration or subtracting a configured Acquisition Delay value.

Acknowledgements

The authors declare that there is no conflict of interest. We would like to thank the JOA reviewers for providing comments that lead to an improvement of the paper.

References

[1] IOTA-VTI http://videotimers.com/home.html
[2] QHY174M-GPS https://www.qhyccd.com/index.php?m=content&c=index&a=show&catid=94&id=46&cut=1
[3] Barry, M. A. Tony, et al., A Digital Video System for Observing and Recording Occultations, Publications of the Astronomical Society of Australia, Volume 32, id.e031 8 pp.
[4] Beisker, W., A Fast Digital CCD Camera with Precise Time-Stamping for Use in Occultation Astronomy and Photometry, EPSC-DPS Joint Meeting 2019, held 15-20 September 2019 in Geneva, Switzerland
[5] Schweizer, A., Meister, S., DVTI, ESOP-38 Paris, https://lesia.obspm.fr/lucky-star/esop38/doc/C1-3-A.Schweizer-S.Meister.pdf
[6] Acquiring High-Resolution Time Stamps https://docs.microsoft.com/en-us/windows/win32/sysinfo/acquiring-high-resolution-time-stamps
[7] GetSystemTimePreciseAsFileTime, https://docs.microsoft.com/en-us/windows/win32/api/sysinfoapi/nfsysinfoapi-getsystemtimepreciseasfiletime
[8] Microsecond Resolution Time Services for Windows http://www.windowstimestamp.com/description
[9] Crystal Oscillators (electronics) https://en.wikipedia.org/wiki/Crystal_oscillator
[10] Intel Software Developer Manual, section 17, page 17-42 https://software.intel.com/sites/default/files/managed/a4/60/325384-sdm-vol-3abcd.pdf
[11] One Windows Kernel https://techcommunity.microsoft.com/t5/Windows-Kernel-Internals/One-Windows-Kernel/ba-p/267142
[12] OccuTimeCheck http://www.hristopavlov.net/OccuTimeCheck.zip
[13] SetSystemTime https://docs.microsoft.com/en-us/windows/win32/api/sysinfoapi/nf-sysinfoapi-setsystemtime
[14] SetSystemTimeAdjustment https://docs.microsoft.com/en-us/windows/win32/api/sysinfoapi/nfsysinfoapisetsystemtimeadjustment
[15] RFC5905 https://tools.ietf.org/html/rfc5905.html
[16] NTPv4 Thresholds http://doc.ntp.org/current-stable/clock.html#step
[17] OccuRec http://www.hristopavlov.net/OccuRec/
[18] Dimension4 https://dimension-4.en.softonic.com/
[19] NetTime http://www.timesynctool.com/
[20] Meinberg NTP https://www.meinbergglobal.com/english/sw/ntp.htm
[21] Tangra http://www.hristopavlov.net/Tangra3/
[22] All graphs from the recorded data are available on: http://www.hristopavlov.net/ntpdata
[23] Windows Time - Support boundary for high-accuracy time, https://docs.microsoft.com/en-us/windows-server/networking/windows-time-service/support-boundary
[24] RFC1361 https://tools.ietf.org/html/rfc1361
[25] Taylor D., Wi-Fi versus a direct connection comparison, http://www.satsignal.eu/ntp/Win-7-Wi-Fi-vs-LAN.html
[26] Gault D., Herald D., All-Of-System Time Testing Using Lunar Occultations, Journal for Occultation Astronomy, No. 2020-01, Vol. 10 No. 1, p. 9-13
[27] The Raspberry Pi as a Stratum-1 NTP Server, https://www.satsignal.eu/ntp/Raspberry-Pi-NTP.html

Beyond Jupiter

The World of Distant Minor Planets

Since the downgrading of Pluto in 2006 by the IAU, the planet Neptune marks the end of the zone of planets. Beyond Neptune, the world of icy large and small bodies, with and without an atmosphere (called Trans Neptunian Objects or TNOs) starts. This zone between Jupiter and Neptune is also host to mysterious objects, namely the Centaurs and the Neptune Trojans. All of these groups are summarized as "distant minor planets". Occultation observers investigate these members of our solar system, without ever using a spacecraft. The sheer number of these minor planets is huge. As of 2020 April 1st, the *Minor Planet Center* listed 1129 Centaurs and 2504 TNOs.

In the coming years, JOA wants to portray a member of this world in every issue; needless to say not all of them will get an article here. The table shows you where to find the objects presented in former JOA issues. (KG)

No.	Name	Author	Link to Issue
944	Hidalgo	Oliver Klös	JOA 1 2019
5145	Pholus	Konrad Guhl	JOA 2 2016
8405	Asbolus	Oliver Klös	JOA 3 2016
10199	Chariklo	Mike Kretow	JOA 1 2017
15760	Albion	Nikolai Wünsche	JOA 4 2019
20000	Varuna	Andre Knöfel	JOA 2 2017
28728	Ixion	Nikolai Wünsche	JOA 2 2018
50000	Quaoar	Mike Kretlow	JOA 1 2020
54598	Bienor	Konrad Guhl	JOA 3 2018
60558	Echeclus	Oliver Klös	JOA 4 2017
90482	Orcus	Konrad Guhl	JOA 3 2017
120347	Salacia	Andrea Guhl	JOA 4 2016
134340	Pluto	Andre Knöfel	JOA 2 2019
136108	Haumea	Mike Kretlow	JOA 3-2019
136199	Eris	Andre Knöfel	JOA 1 2018
136472	Makemake	Christoph Bittner	JOA 4 2018

In this Issue:

(2060) Chiron

Mike Kretlow • IOTA/ES • Lauenbrück • Germany • mike@kretlow.de

ABSTRACT: (2060) Chiron aka 95P/Chiron is a large Centaur showing cometary activity and possibly hosts a ring system. Comparisons to both 29P/Schwassmann-Wachmann 1 (outbursts) and (10199) Chariklo (ring system) are obvious. Centaurs are regarded as small bodies, moving in unstable, non-resonant, orbits between Jupiter and Neptune, and being in a transition phase between Trans-Neptunian Objects (TNO) and other populations of the inner Solar System, notably Jupiter-Family Comets (JFC). Chiron is one target of a proposed NASA Discovery programme mission named Centaurus.

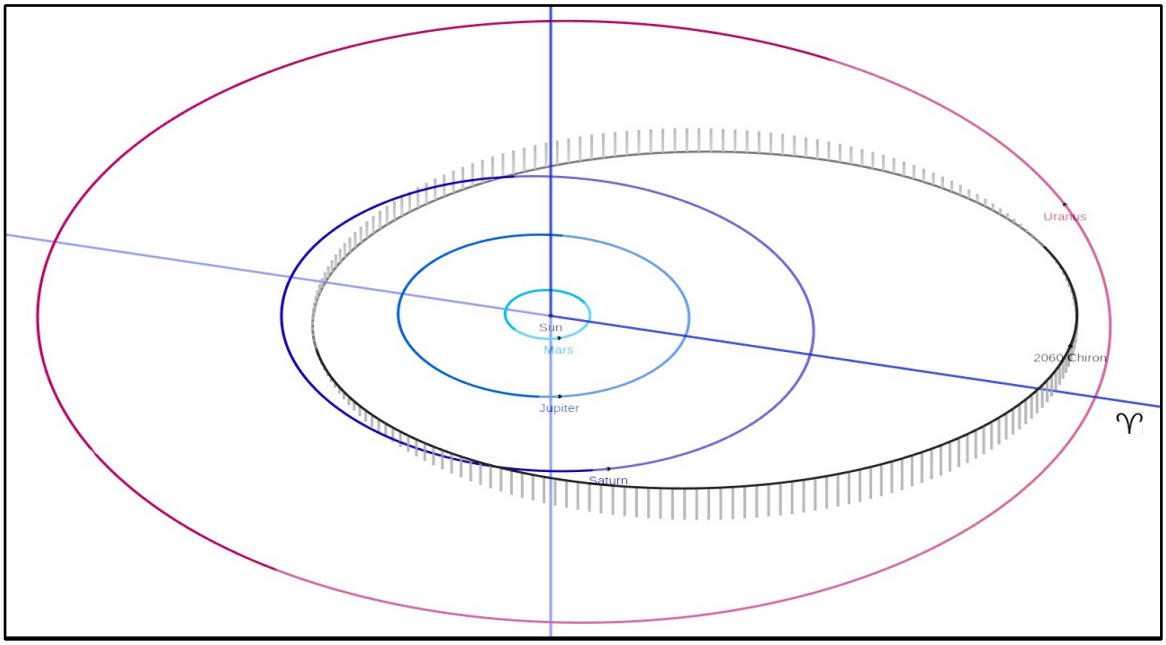

Figure 1. Orbit and position of (2060) Chiron and some outer planets as seen from an oblique perspective above the ecliptic plane for the date 01 June 2020. Chiron's distance to the Earth and to the Sun for this date is 19.30 AU and 18.85 AU, respectively. Figure made with JPL's Small-Body Database Browser, https://ssd.jpl.nasa.gov/sbdb.cgi?sstr=2060 .

Introduction

Centaurs are small bodies of our Solar System moving around the Sun between Jupiter and Neptune on unstable, non-resonant, orbits, because they cross (or crossed) the orbit of one or more of the giant planets. Their dynamical mean lifetime is short (~10^{5-7} yr) [1, 2]. They are assumed to be in a transition phase between Trans-Neptunian Objects (TNO) and other populations of the inner Solar System, particularly Jupiter-Family Comets (JFC), though this relationship and the transition process is not well studied. They can also be transported outward or even ejected from the Solar System [2]. Beside this more generic definition of Centaurs as bodies orbiting the Sun between Jupiter and Neptune in a non-resonant orbit, several more specific classifications exist in the scientific community and / or literature. The Minor Planet Center (MPC) for example defines Centaurs as objects having perihelia q beyond the orbit of Jupiter and semi-major axes a inside the orbit of Neptune, whereas the Jet Propulsion Laboratory (JPL) just restricts the semi-major axis a to be between those of Jupiter and Neptune (5.5 AU $\leq a \leq$ 30.1 AU). Currently several hundred Centaurs are known[1]. The whole population of Centaurs more than 1 km in diameter might range from 10^4 up to 10^7 [2, 3].

Beside their dynamical life history, Centaurs are remarkable and interesting objects, because they can have cometary activity, brightness outbursts, satellites and even rings. The largest currently known Centaur is (10199) Chariklo [4], with a mean diameter of about 250 km [5].

[1] The MPC lists Centaurs and Scattered-Disk Objects in one table which currently numbers 951 objects as of 05 Feb. 2020.

Discovery and Name

Chiron was discovered by Charles T. Kowal on photographic plates taken on October 18 and 19, 1977, with the 122-cm Schmidt telescope at Palomar Observatory and first announced as "slow-moving object Kowal" on 4 November 1977. It was given the provisional designation 1977 UB. Later, pre-discovery images going back to 1895 were found. At the time of discovery it was the most distant known minor planet – the first Trans-Neptunian Object (TNO) was discovered 15 years later. In April 1978 the object was numbered and named (2060) Chiron, after the most important Centaur from Greek mythology, a half-human, half-horse creature. In the official naming citation published by the Minor Planet Center (MPC) it was suggested to reserve names of these mythological Centaurs to this population of objects. Nevertheless it should be noted that (2060) Chiron is not the first ever discovered Centaur. (944) Hidalgo, discovered in 1920 by German astronomer Walter Baade at Bergedorf Observatory near Hamburg, Germany, belongs to the Centaurs as well [6]. But at that time Hidalgo was considered to be a (maybe somehow special) asteroid, because this population of objects was not recognized as a distinct class until the discovery of Chiron. Hidalgo was named after the Mexican revolutionary Miguel Hidalgo y Costilla (1753-1811).

Orbit

Chiron moves around the Sun in about 50 years, primarily between the orbits of Saturn and Uranus, with heliocentric distances ranging between 8.5 AU and 19 AU in a quite eccentric (e = 0.37) and moderately inclined (i = 7°) orbit (Figure 1). Chiron's last perihelion occurred in 1996, the next aphelion will be in 2021.

Physical Characteristics

Chiron's rotational period has been reported as P = 5.918 h, the light curve amplitude as 0.04-0.09 mag [7]. In 1988 an anomalous brightness increase by 0.6 mag in February / March and 1.0 mag in September / October was observed [8], which violates the brightness formula used for asteroids; this behaviour is more typical for comets. At that time Chiron was ~12.5 AU from the Sun (compared to r ~18 AU at the time of discovery in 1977). In 1989 a coma around Chiron was detected [8], and finally a tail in 1993. It was hypothesized that Chiron is an (unusual large) comet with outbursts perhaps similar to those observed for comet 29P/Schwassmann-Wachmann 1 (which is meanwhile also classified as a Centaur). These circumstances led to a co-designation as comet 95P/Chiron. Meanwhile, Chiron is the namesake of the Chiron-type comet family (CTC), having (as defined by Levison and Duncan) a semi-major axis larger than that of Jupiter (a > 5.2 AU) and a Tisserand parameter[2] T_J > 3. Stellar occultations revealed an asymmetric dust coma as well as discrete jet-like features. Chiron's size was estimated with different methods like stellar occultations, thermal observations by *IRAS*, *Spitzer* and *Herschel*, and also with *ALMA* (Atacama Large Millimetre/submillimetre Array), ranging from 160 km (lower limit) up to 270 km spherical diameter. Chiron's visible to near-infrared spectrum is neutral, and water ice has been detected [9].

On 29 November 2011, (2060) Chiron occulted a R ~15-mag star as observed from the 3-m NASA Infrared Telescope Facility (IRTF) on Mauna Kea and the 2-m Faulkes Telescope North (FTN) at Haleakala (Figure 2). Data were taken as visible wavelength images and simultaneous, low-resolution, near-infrared (NIR) spectra (Figure 3). Before and after the main body occultation, dips were detected in the occultation light curve (in about 300 km in-skyplane distance from Chiron's centre), which can be interpreted as an arc or shell of material around Chiron [10], or as a (full) ring system [11, 12], similar to the rings around the Centaur (10199) Chariklo, which were discovered by stellar occultation in 2013.

[2] Tisserand's parameter with respect to Jupiter as perturbing body is frequently used to distinguish asteroids (typically T_J > 3) from Jupiter-family comets (typically 2 < T_J < 3).

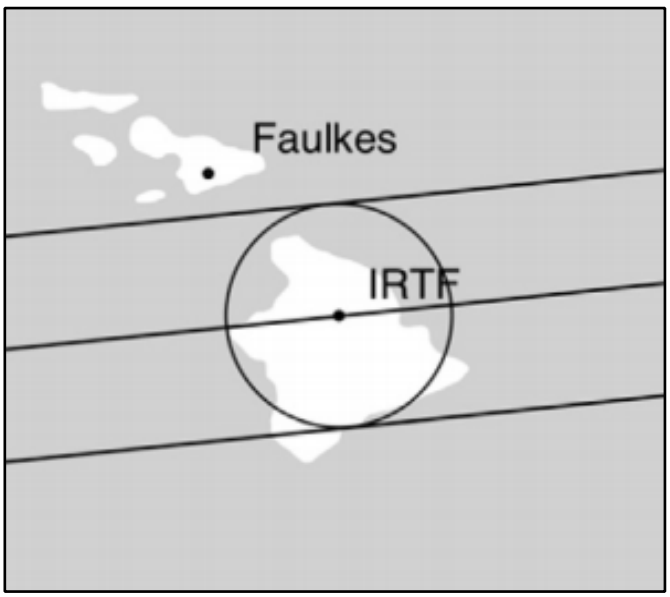

Figure 2. Chiron's approximate occultation shadow (prediction with an assumed diameter of 180 km) path over Hawaii [10].

Exploration

In 2010 a *Chiron Orbiter Mission* study was published with possible launch dates between 2019 and 2025 [13]. Later in 2019 another mission concept named *Centaurus* was submitted to NASA's Discovery 15 and 16 mission proposal call [14, 15]. *Centaurus* is a fly-by mission proposed to study (2060) Chiron and 29P/Schwassmann-Wachmann 1, another well-known Centaur about 60 km in diameter, famous for its cometary outbursts, and also an attractive target for study by the stellar occultation technique [16]. Possible launch of *Centaurus* could be between 2026 and 2029.

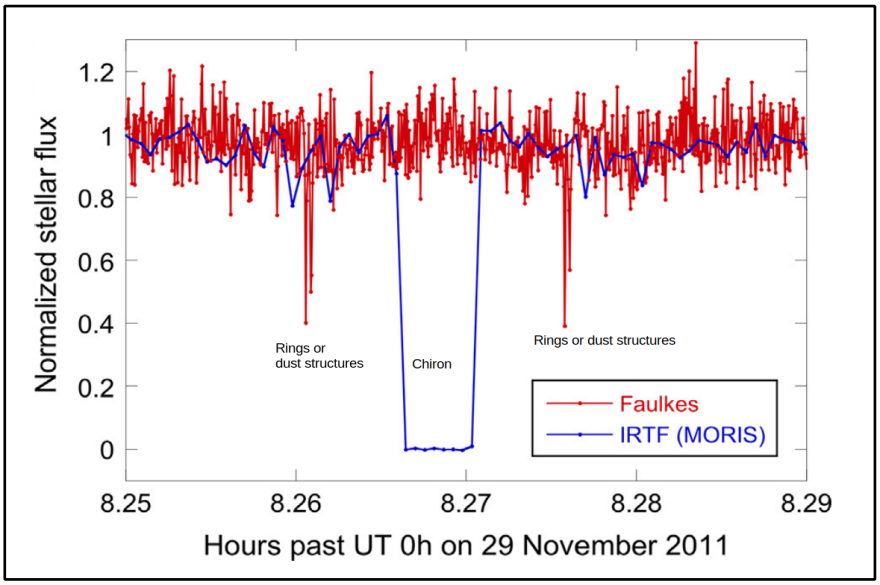

Figure 3. On 29 November 2011, (2060) Chiron occulted a R = 14.9-mag star. Data were successfully obtained at the 3-m NASA Infrared Telescope Facility (IRTF) on Mauna Kea and the 2-m Faulkes Telescope North (FTN) at Haleakala. Besides the solid-body detection of Chiron's nucleus at IRTF with a chord duration of 16.0 ± 1.4 s, corresponding to a chord length of 158 ± 14 km, symmetric, dual extinction features in the FTN light curve indicate the presence of optically thick material roughly 300 km from the body midpoint. Figure modified from [10].

References

[1] Fernández J. A., Helal, M. and Gallardo, T. Dynamical evolution and end states of active and inactive Centaurs. Planetary and Space Science, vol. 158, 6–15. (2018)

[2] Horner, J., Evans, N. W. and Bailey, M. E. Simulations of the population of Centaurs - I. The bulk statistics. Monthly Notices of the Royal Astronomical Society, vol. 354, 798–810. (2004)

[3] Sarid, G., Volk, K., Steckloff, J. K., Harris, W., Womack, M. and Woodney, L. M. 29P/Schwassmann-Wachmann 1, A Centaur in the Gateway to the Jupiter-family Comets. The Astrophysical Journal Letters, vol. 883, L25. (2019)

[4] Kretlow, M. Beyond Jupiter: (10199) Chariklo. Journal for Occultation Astronomy, vol. 7, no. 1, 7–11. (2017)

[5] Leiva R. *et al.* Size and Shape of Chariklo from Multiepoch Stellar Occultations. The Astronomical Journal, vol. 154, 159. (2017)

[6] Klös, O. Beyond Jupiter - (944) Hidalgo. Journal for Occultation Astronomy, vol. 9, no. 1, 20–23. (2019)

[7] LCDB. http://www.minorplanet.info/PHP/GenerateLCDBHTMLPages.php [accessed 6 February 2020].

[8] Hartmann, W. K., Tholen, D. J., Meech, K. J. and Cruikshank, D. P. 2060 Chiron - Colorimetry and cometary behavior. Icarus, vol. 83, 1–15. (1990)

[9] Luu, J. X., Jewitt, D. C. and Trujillo, C. Water Ice in 2060 Chiron and Its Implications for Centaurs and Kuiper Belt Objects. The Astrophysical Journal Letters, vol. 531, L151–L154. (2000)

[10] Ruprecht, J. D. *et al.* 29 November 2011 stellar occultation by 2060 Chiron: Symmetric jet-like features. Icarus, vol. 252, 271–276. (2015)

[11] Sickafoose, A. A. *et al.* Characterization of material around the centaur (2060) Chiron from a visible and near-infrared stellar occultation in 2011. Monthly Notices of the Royal Astronomical Society, vol. 491, 3643–3654. (2020)

[12] Ortiz, J. L. *et al.* Possible ring material around centaur (2060) Chiron. Astronomy and Astrophysics, vol. 576, A18. (2015)

[13] Buie, M. Chiron Orbiter Mission, *NASA Solar System Exploration*. https://solarsystem.nasa.gov/studies/224/chironorbitermission [accessed 5 February 2020].

[14] Singer, K. and Stern, S. A. Centaurus: A Spacecraft Discovery Mission Proposal to Explore Centaurs and More, Messengers from the Era of Planet Formation. (2019) https://figshare.com/articles/Centaurus_A_Spacecraft_Discovery_Mission_Proposal_to_Explore_Centaurs_and_More_Messengers_from_the Era_of_Planet_Formation/9956210.

[15] Singer, K. N., Stern, S. A., Stern, D., Verbiscer, A. and Olkin, C. Centaurus: Exploring Centaurs and More, Messengers from the Era of Planet Formation. https://meetingorganizer.copernicus.org/EPSC-DPS2019/EPSC-DPS2019-2025.pdf.

[16] Miles; R. and Kretlow, M. Studying Comets by the Stellar Occultation Method. Journal for Occultation Astronomy, vol. 8, no. 1, 11–13. (2018)

Further Reading

Peixinho, Nuno; Thirouin, Audrey; Tegler, Stephen C.; Di Sisto, Romina; Delsanti, Audrey; Guilbert-Lepoutre, Aurélie; Bauer, James G., "From Centaurs to Comets - 40 years.", 2020, Review chapter to be published in the book "The Transneptunian Solar System", Editors: Dina Prialnik, Maria Antonietta Barucci, and Leslie Young, Publisher: Elsevier (20 pages, 2 figures, 1 long table); doi:10.1016/B978-0-12-816490-7.00014-X, arXiv:1905.08892.

Breaking News

The 14th Trans-Tasman Symposium on Occultations Goes Virtual on 2020 April 13

2020 April 02

Steve Kerr, RASNZ Occultation Section Director, announces: *"With the COVID-19 corona virus severely restricting the movement of people pretty much everywhere across the world, the Australian NACAA (National Australian Convention of Amateur Astronomers) was cancelled some weeks ago and with it the proposed 14th Trans-Tasman Symposium on Occultations (TTSO14). Thanks to the efforts of our speakers and RASNZ Occultation Section members, we have managed to salvage a program to run in an entirely on-line forum similar to how previous TTSO's have been webcast. We are using the same MeetCheap platform as we have used before and while that has its limitations, testing so far would suggest that we can run a useful conference given some patience as we switch between speakers."*
Details on how to connect to the webcast: http://www.occultations.org.nz/meetings/TTSO14/TTSO14.htm

Figure 1. Main building of the Archenhold-Sternwarte in Berlin-Treptow, Germany, with the 'Large Refractor'. The IOTA/ES workshop was held inside the lecture room of the 5-metre dome in the garden of this historic site.

IOTA/ES-Workshop QHY174M-GPS

Oliver Klös • IOTA/ES • Eppstein-Bremthal • Germany • pr@iota-es.de

ABSTRACT: On 2020 February 29th participants from the Czech Republic, Poland and Germany met at Archenhold Sternwarte in Berlin to practice how to use the QHY174M-GPS camera. Dr. Christian Weber, IOTA/ES, had made several tests in the weeks before the workshop and presented the basic and advanced settings for this camera with SharpCap software. The participants learned that this camera is not a 'plug & play' device.

Introduction

The QHY174M-GPS camera [1] is a digital camera for astronomical measurements with an integrated GPS module for accurate timing and was used to record an occultation by (486958) Arrokoth [2]. Therefore it presents a major step from analogue video timing into the digital age for occulation work. Because this camera will now be used by some members of IOTA/ES, in January 2020 the association invited members and non-members to Berlin for a workshop about the calibration and the use of this camera.

The 11 occultation observers who met in the lecture room in the building of the 5-metre dome in the garden of the Archenhold-Sternwarte (Figure 1), were on different experience levels. In the invitation Christian Weber recommended everyone to bring their own cameras and computers to the workshop to have practical experiences first hand. The operating systems of the computers ranged from *Windows 7* to *10,* the cameras were from different production stages and were supplied with different GPS antennas.

Some of the participants had already made some occultation recordings with the new camera, some had just connected the new imaging system to their computers. During the following hours it was obvious that using their own equipment was an important recommendation.

First Part - Basic Use

In the first part of the workshop Christian Weber gave a presentation of 'what's in the box' and solved some mysteries of the supplied cables and parts provided with the camera by QHY. The installation of the software *SharpCap* by Robin Glover [3] was shown step by step and an overview of the camera settings was given. The participants connected their computers to their cameras and GPS antennas and gave it a try with the recommended settings at first hand. The benefits for occultation work of the PRO-version of *SharpCap* were demonstrated.

Second Part - Advanced Use

Additional recommended software such as *PyMOVIE [4]*, *PyOTE [5]* and *Tangra [6]* were mentioned but it was not possible to get deeper into this because of time restrictions. The SEXTA device donated by Dave Gault was sent from Paris to check the reliability of the time stamps of the camera [7]. Christian Weber measured an accuracy of < 2 ms.

Christian Weber presented which five parameters will affect GPS calibration if they are changed. These parameters are dynamic range (8/16 bit) , binning, the height of the region of interest (ROI), exposure time and USB-traffic. The GPS calibration with the built-in LED close to the sensor of the camera was demonstrated with a brand new calibration feature of *SharpCap*. The homework given to the participants was to set up different files with different settings of the critical parameters and calibrate each of them individually. This is essential to make fast changes when needed during occultation measurements, e.g. if the exposure time has to be changed due to thin clouds.

Summary

The workshop led to a fruitful exchange and discussion about the camera and the capture software. It was much easier to unlock the secrets of the settings during this personal meeting than by discussing topics via e-mail. All participants agreed that the camera can not be used 'out of the box' in a 'plug & play' manner for accurate timing measurements and that the instructions provided by QHY are very limited.

The presentations are now available on the IOTA/ES webpage [8]. A worksheet in PDF format for all users of this camera will be provided by Christian Weber in the near future. Its publication will be announced by IOTA/ES. This worksheet will be revised when new relevant features of *SharpCap* for occultation work are released.

Acknowledgements

Many thanks to...
Christian Weber, who has spent many hours to fine tune the setting for this camera and to check its reliability.
Robin Glover, who has already improved *SharpCap* for occultation work and will stay in contact with Christian Weber for additional features.
Sven Andersson, Konrad Guhl and Nikolai Wünsche, the LOC at Archenhold Sternwarte, for providing the location of the workshop.

References

[1] Webpage of QHY174M-GPS https://www.qhyccd.com/index.php?m=content&c=index&a=show&catid=94&id=46
[2] Buie, M. *et al.* Size and Shape Constraints of (486958) Arrokoth from Stellar Occultations, arXiv:2001.00125 [astroph.EP], (2020)
[3] Glover, R. SharpCap https://www.sharpcap.co.uk/ (2020)
[4] Anderson, B. PyMOVIE http://occultations.org/observing/software/pymovie/ (2019)
[5] Anderson, B. PyOTE http://occultations.org/observing/software/ote/ (2019)
[6] Pavlov, H. Tangra http://www.hristopavlov.net/Tangra3/ (2018)
[7] Gault, D. SEXTA http://www.kuriwaobservatory.com/SEXTA/SEXTA.html, (2019)
[8] Weber, C. IOTA/ES Workshop QHY174M-GPS, http://www.iota-es.de/qhy174gps_workshop.html, (2020)

Figure 2. Christian Weber shows a diagram about data reduction during the first part of the presentations. The particpants have their setups already running (counterclockwise from left: Miroslav Poláček, Peter Lindner, Nikolai Wünsche, Anna Marciniak, Sven Andersson, Christoph Bittner, Christian Weber and Jan Mánek).

Hal Povenmire

1939 – 2019

Hal Povenmire (left) is awarded with IOTA David E. Laird Award by Steve Preston (centre) and David Dunham in 2013.

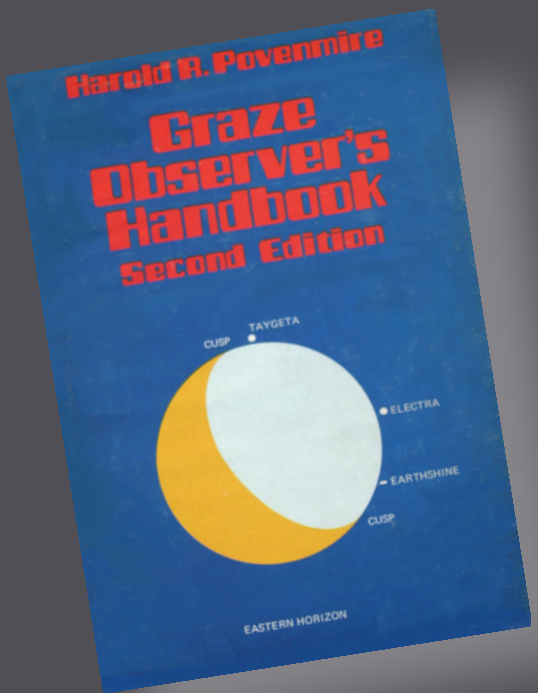

It is with great sorrow, that I announce the passing of an intrepid astronomer, avid occultationist, researcher of tektites, prolific author and great friend.

Hal was born in Columbus, Ohio. He had a Bachelor and Masters degree in Science from Ohio State University and another degree in Technology Specialist from the Florida Institute of Technology. He was part of the Apollo missions 8, 10 and 11. He wrote numerous books on Tektites, Occultations, and most recently on UFOs. He also wrote a book on musings and experiences with NASA. Asteroids (12753) Povenmire and (15146) HalPov honour Hal and Katie Povenmire for their contributions to planetary astronomy. Hal accomplished the feat of having observed over 500 grazes during his lifetime! In 2013, Hal was awarded the I.O.T.A. David E. Laird Award for making significant contributions to occultation science and to the work of IOTA.

I first met Hal in 1990 at the Texas Star Party. He had a table set up with some of his books for sale, and was answering general questions about tektites and occultations. We had a fairly long discussion about both. We then kept in communication by written letters and e-mails.

In July of 2005 Hal invited me and my wife to come join him and Katie in Flagstaff, Arizona. We spent the week mostly sight seeing. Hal knew some of the people at Lowell Observatory and got us passes to participate in the Discovery Telescope dedication happening that week. Later Hal took me up on "the hill" to meet some of the astronomers he knew and watch them do their nightly runs at the telescope.

Hal was very old school when it came to things like calculators and computers. I don't think he ever used either one. While in Flagstaff, we visited the USGS office to get some topographical maps so he could plot some upcoming grazes in which he had an interest. They copied the maps full scale and he took them over to a table to start computing and plotting the graze. He did this not with a calculator but with a slide rule! I asked him why not a calculator and his reply was he did not trust them.

Over the course of the following years, Hal called me at least once a month to check up to see how I was doing and usually request predictions for grazes or total occultations. I would do the run using *Occult* and e-mail him copies through Katie's e-mail account. Remember I said he was old school. I don't think he ever touched a computer. Katie would print the predictions and e-mails that I sent him.

The last time I saw Hal was around 2008(?). He was travelling though Kansas City, stopped and picked up Bob Sandy in Blue Springs MO and ended up at my place to visit. Hal, Katie and Bob spent about an hour and then they were on their way. He referred to me, Bob and himself as the "three amigos".

Over the years we spent much time not only talking about science but world problems and current news. Although we did not agree on all things, we both appreciated and respected each other's opinions. He always ended up the discussion with "now that we have solved all the world's problems, have you heard the joke about..." He was always that way. Serious stuff first and finishing up with humour.

Hal never discussed any of his health problems, but I suspected he knew something was amiss when in 2015 he started talking about all the graze reports he had never submitted and wanted to make sure they were recorded before "he dropped off the face of the Earth", as he put it. Over the course of 3-4 months, he sent me I believe around 70 observation reports which I entered into *Occult*, reduced and sent to David Herald for proofing and archiving. I had no idea at the time he was having heart and diabetes issues. He did mention at one time that he and doctors thought he had a small stroke but that it was not debilitating. He claimed sometimes he had short term memory loss, but attributed it to old age.

The last time I talked to Hal was just after Thanksgiving, 2019. He called and was all excited about the upcoming asteroid occultation by Pandora which was going to pass over Jacksonville, Florida. I sent him detailed predictions, maps, and other pertinent information. It was ironic that the same evening that he would have been observing that event, was the same day he passed away (Dec 6th, 2019).

Hal will be sadly missed.

Walt "Rob" Robinson
Vice-President of Occultation Services IOTA

Hal Povenmire at the Discovery Telescope dedication happening in 2005.

The "Three Amigos" - Bob Sandy, Hal Povenmire and Walt "Rob" Robinson (left to right)

Journal for Occultation Astronomy

IOTA's Mission

The International Occultation Timing Association, Inc was established to encourage and facilitate the observation of occultations and eclipses It provides predictions for grazing occultations of stars by the Moon and predictions for occultations of stars by asteroids and planets, information on observing equipment and techniques, and reports to the members of observations made.

The Journal for Occultation Astronomy (JOA) is published on behalf of IOTA, IOTA/ES and RASNZ and for the worldwide occultation astronomy community.

Worldwide Partners

Club Eclipse (France). . . . . www.astrosurf.com/club_eclipse
IOTA-India . . . . . http://iota-india.in
IOTA/ME (Middle East) . . . . . www.iota-me.com
President: Atila Poro . . . . . iotamiddleeast@yahoo.com
LIADA (Latin America) . . . . . www.ocultacionesliada.wordpress.com
SOTAS (Stellar Occultation Timing Association Switzerland) . . . . . www.occultations.ch

Imprint

Editorial Board: Wolfgang Beisker, Oliver Klös, Mike Kretlow, Alexander Pratt
Responsible in Terms of the German Press Law (V.i.S.d.P.): Konrad Guhl

Publisher: IOTA/ES, Am Brombeerhag 13, D-30459 Hannover Germany, e-mail: joa@iota-es.de

Layout Artist: Oliver Klös Original Layout by Michael Busse (†)
Webmaster: Wolfgang Beisker, wbeisker@iota-es.de

Membership Fee IOTA/ES: 20,– Euro a year

Publication Dates: 4 times a year

Submission Deadline for JOA 2020-3: May 15

IOTA maintains the following web sites for your information and rapid notification of events:

www.occultations.org
www.iota-es.de
www.occultations.org.nz

These sites contain information about the organisation known as IOTA and provide information about joining.

The main page of occultations.org provides links to IOTA's major technical sites, as well as to the major IOTA sections, including those in Europe, Middle East, Australia/New Zealand, and South America.

The technical sites hold definitions and information about all issues of occultation methods. It contains also results for all different phenomena. Occultations by the Moon, by planets, asteroids and TNOs are presented. Solar eclipses as a special kind of occultation can be found there as well results of other timely phenomena such as mutual events of satellites and lunar meteor impact flashes.

IOTA and IOTA/ES have an on-line archive of all issues of Occultation Newsletter, IOTA'S predecessor to JOA.

Journal for Occultation Astronomy

(ISSN 0737-6766) is published quarterly in the USA by the International Occultation Timing Association, Inc. (IOTA)
PO Box 423, Greenbelt, MD 20768

IOTA is a tax-exempt organization under sections 501(c)(3) and 509(a)(2) of the Internal Revenue Code USA, and is incorporated in the state of Texas. Printed Circulation: 200

Regulations

The Journal of Occultation Astronomy (JOA) is not covenanted to print articles it did not ask for.

The author is responsible for the contents of his article & pictures.

If necessary for any reason JOA can shorten an article but without changing its meaning or scientific contents.

JOA will always try to produce an article as soon as possible based to date & time of other articles it received – but actual announcements have the priority!